iScience

CellPress

Article

A High-Quality Melon Genome Assembly Provides Insights into Genetic Basis of Fruit Trait Improvement

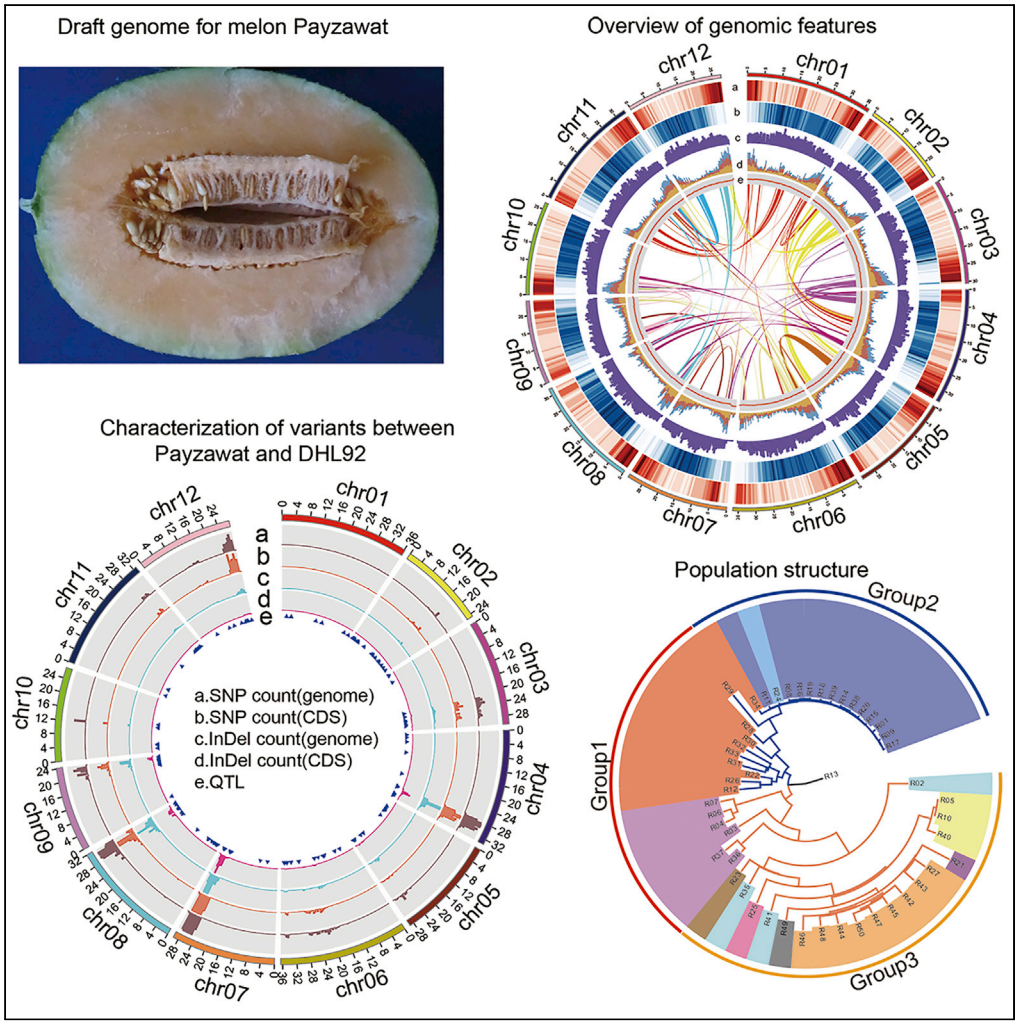

Hong Zhang, Xuming Li, Haiyan Yu, ..., Jianshun Miao, Hongkun Zheng, Hongping Yi

zhenghk@biomarker.com.cn (H.Z.)
hpyi1223@163.com (H.Y.)

HIGHLIGHTS

Provides a high-quality assembly for melon genome

Explains a considerable proportion of epidermis thickness

Melons in China are introduced from different routes

Haplotypes of alleles associated with agronomic traits enable efficient breeding

DATA AND CODE AVAILABILITY

SUB4523929

Zhang et al., iScience 22, 16–27
December 20, 2019
https://doi.org/10.1016/j.isci.2019.10.049

iScience

CellPress

Article

A High-Quality Melon Genome Assembly Provides Insights into Genetic Basis of Fruit Trait Improvement

Hong Zhang,[1,4] Xuming Li,[3,4] Haiyan Yu,[3,4] Yongbing Zhang,[1] Meihua Li,[1] Haojie Wang,[1] Dengming Wang,[1] Huaisong Wang,[2] Qiushi Fu,[2] Min Liu,[3] Changmian Ji,[3] Liming Ma,[3] Juan Tang,[3] Song Li,[3] Jianshun Miao,[3] Hongkun Zheng,[3,*] and Hongping Yi[1,5,*]

SUMMARY

Accurate reference genomes have become indispensable tools for characterization of genetic and functional variations. Here we generated a high-quality assembly of the melon Payzawat using a combination of short-read sequencing, single-molecule real-time sequencing, Hi-C, and a high-density genetic map. The final 12 chromosome-level scaffolds cover ~94.13% of the estimated genome (398.57 Mb). Compared with the published DHL92 genome, our assembly exhibits a 157-fold increase in contig length and remarkable improvements in the assembly of centromeres and telomeres. Six genes within *STHQF12.4* on pseudochromosome 12, identified from whole-genome comparison between Payzawat and DHL92, may explain a considerable proportion of the skin thickness. In addition, our population study showed that melon domesticated at multiple times from whole-genome perspective and melons in China are introduced from different routes. Selective sweeps underlying the genes related to desirable traits, haplotypes of alleles associated with agronomic traits, and the variants from resequencing data enable efficient breeding.

INTRODUCTION

Melon (*Cucumis melo* L.) is an economically important crop. The annual yield is estimated to be about 30 million tons worldwide, with China contributing to more than half of global melon production (http://www.fao.org). Melon is a eudicot diploid plant species (2n = 2x = 24), belonging to the Cucurbitaceae family. Melon is cultivated worldwide and mainly grows in temperate, subtropical, and tropical regions.

Cucumis melo L. is classified into two sub-species: melo and agrestis. The origin of *C. melo* remains controversial as wild relatives can be found in Africa and Asia (Diaz et al., 2017). The sub-species agrestis is found mainly in Asia from India to the Far-East and in Africa and Central America. The sub-species melo is found in India, Central and Western Asia, Africa, Europe, and America (Pitrat, 2013). Wild melons are observed in these two sub-species. Until recently, independent domestication of wild melons in Africa and Asia resolved the geographic origin of melon (Endl et al., 2018). The traits in fruit morphology and quality are diverse in different horticultural groups. The wild and cultivated melons show contrasting phenotypic traits. The fruit, flower, and seed of wild melons are small, and the plant is monoecious. The fruit of wild melons is bitter, differing from the sweetness of cultivar melons. These are domestication traits and evidently different in wild and cultivar accessions.

The draft genome of melon was released in 2012 (Garcia-Mas et al., 2012); however, it was sequenced using the short reads, resulting in a highly fragmented genome assembly. Although efforts had been made to anchor the genome into pseudochromosomes using genetic maps (Argyris et al., 2015), their marker coverage was not sufficient to anchor many gene-rich scaffolds or correct mistakes made in the genome assembly. Moreover, short-read sequencing has difficulty in traversing complex repeat structures, leading to incomplete gene models, less accurate representation of repeats, and biases in our understanding of genome biology (Gordon et al., 2016). The lack of an accurate genome assembly also hinders many studies that rely on genome sequences, such as resequencing, transcriptome, and genetic mapping. Until now, the current version of melon genome (v3.6.1) for DHL92 has more than 40,000 sequence gaps (Ruggieri et al., 2018), making it highly fragmented.

[1]Hami Melon Research Center, Xinjiang Academy of Agricultural Sciences, Urumqi, Xinjiang 830091, China

[2]The Institute of Vegetables and Flowers, Chinese Academy of Agricultural Sciences, Beijing 100081, China

[3]Biomarker Technologies Corporation, Beijing 101200, China

[4]These authors contributed equally

[5]Lead Contact

*Correspondence: zhenghk@biomarker.com.cn (H.Z.), hpyi1223@163.com (H.Y.)

https://doi.org/10.1016/j.isci.2019.10.049

The single-molecule real-time (SMRT) sequencing technology allows researchers to obtain long reads with tens of kilobases in size that can span repeat-rich genomic regions, thus significantly reducing sequencing gaps. The completeness of a variety of genome assemblies have been improved by using the SMRT technology, such as quinoa (Jarvis et al., 2017), goat (Bickhart et al., 2017), gorilla (Gordon et al., 2016), and citrus (Wang et al., 2017). In this study, we combined the SMRT sequencing and high-throughput chromosome interaction mapping (Hi-C) technologies to obtain a high-quality genome assembly of a cultivated melon species named Payzawat, a most typical representative of *Cucumis melo* sp. melo in China. Furthermore, resequencing a number of accessions allows a better understanding of the evolution of melon and provides candidate genes controlling phenotypic traits involved in domestication or diversification.

RESULTS

De Novo Sequencing and Assembly

The SMRT sequencing technologies were used to assemble a high-quality reference genome for melon. A total of 27.80 Gb error-corrected PacBio sub-reads were individually assembled into the contigs with Canu (v1.5) (Koren et al., 2017) assembler and DBG2LOC (Ye et al., 2016), respectively (see Table S2). The resulting two draft assemblies (365 and 389 Mb, see Table S3) then were merged into a consensus assembly. The consensus was polished with PacBio sub-reads and Illumina reads. The estimated genome size for Payzawat was 398.57 Mb using kmer analysis (see Figure S1). As a result, the final genome assembly was 386 Mb with contig N50 and N90 of 2.86 Mb and 511.5 Kb, respectively (see Table S3). This assembly showed substantial improvements compared with the latest assembly of CM3.6.1 (Garcia-Mas et al., 2012), including in terms of assembly completeness, contiguity (gap filling), TE content, etc. With the aid of Hi-C interaction data, 95.53% (363.76 Mb) of the assembly was anchored onto 12 pseudochromosomes (see Table S4 and Figure 1). The Hi-C heatmap of the genome using Hi-C plotter (Akdemir and Chin, 2015) at 200-kb resolution showed the high accuracy of melon assembly (see Figure S2A).

Assembly Assessment

To assess the accuracy of the anchored pseudochromosomes, the genetic markers yielded from an RIL population containing 119 individuals were mapped onto the genome assembly. The results showed that the orders of these markers were highly consistent with the pseudochromosomes (see Figure S2B).

The conserved plant gene sets such as CEG and BUSCO and the specific repeats in melon were also used to evaluate the quality of the genome assembly. A total of 448 (97.82% of 458) CEGs, including 246 (99.19% of 248) highly conserved CEGs, could be found in the melon genome (see Table S7). BUSCO (Simao et al., 2015) assessment showed that 1,336 (92.78%) of gene models were complete, 30 (4.03%) gene models were fragmented, and 76 (5.14%) gene models were missing (Table S8). Melon-specific CentM centromeric repeats (GenBank accession no. 3929695) were found in all 12 chromosomes with a maximum length of 26,811 bp (see Figure S3 and Table S10). In CM3.6.1 genome, centromeric repeats were found only in ten chromosomes with a maximum length of 8,839 bp (see Figure S3 and Table S11). The maximum length of telomeres in Payzawat was 33,998 bp other than 118 bp in CM3.6.1 (see Figure S3 and Tables S12 and S13). In addition, 99.03% of the short reads and 71.82% of the Pacbio sub-reads could be correctly remapped to the assembly with 90.67% and 70% coverage, respectively. All these data verified the high-quality assembly of the Payzawat genome.

Genome Annotation

A total of 192.4 Mb repetitive sequences were identified in Payzawat genome, of which 83.2% (160 Mb) were retrotransposons and 10.02% (38.7 Mb) were DNA transposons (see b in Figure 1 and Table S14).

Protein-coding genes were predicted by integrating evidence from RNA sequencing (RNA-seq)-based prediction, protein-homology-based prediction, and *ab initio* prediction. A total of high-quality 22,924 gene models were predicted in the Payzawat genome (see Table S15 and Figure S4), of which 22,298 (97.27%) genes were supported by RNA-seq or homolog evidence (see Figure S4 and Table S17) and 22,506 (98.18%) could be annotated by at least one of the public databases (see Table S20). The length distributions of mRNA, CDS, and intron were similar to species within the Cucurbitaceae family (see Figures S5A–S5C). The average length of gene model is 4,491 bp (see Tables 1 and S16), and the median length of mRNA is 3,166 bp in Payzawat longer than 2,326 bp in CM3.6.1. The median number of exons is four in Payzawat but three in CM3.6.1 (see Table 1). In total, 22,037 (96%) of protein-coding genes were allocated to 12

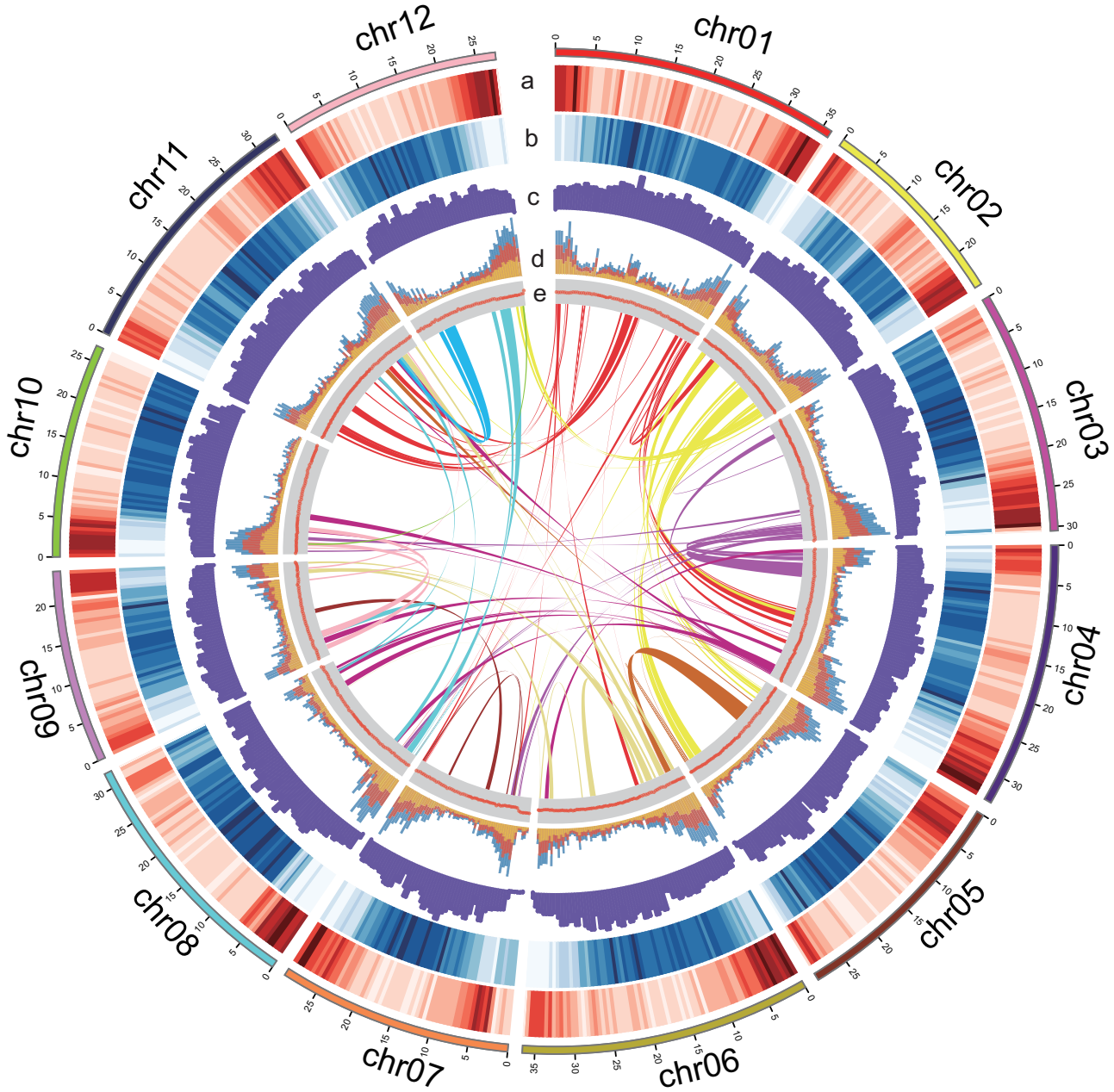

Figure 1. An Overview of the Genomic Features of Payzawat Melon in 500-kb Intervals

The outer layer shows the 12 chromosomes. (a) Gene density. (b) Repeat coverage. (c) SNP density of 50 resequencing accessions. (d) GC content. (e) Duplications of genomic paralogous sequences in melon.

pseudochromosomes. The density of genes tended to be higher and the density of repeats tended to be lower at both ends of the chromosome (see a and b in Figure 1).

Whole-Genome Comparison between Payzawat and CM3.6.1 Genome

Genomic collinearity analysis between Payzawat and CM3.6.1 revealed that 76.7% (296.59 Mb) of Payzawat genomes have one-to-one syntenic blocks with 71.1% (296.29 Mb) of CM3.6.1, and these syntenic blocks accommodated 83.36% (19,110) of genes in Payzawat and 89.63% (26,869) in CM3.6.1, respectively (see Figure 2, and Table S23 and Figure S6).

	Payzawat (*C. melo* L. cv. inodorus)	DHL92 (*C. melo* L. cv. DHL92, CM3.6.1)
Number of genes	22,924	29,980
Number of mRNAs	22,924	29,980
Number of 5′UTR	17,419	23,703
Number of 3′UTR	16,078	22,546
Median mRNA length	3,166	2,326
Median CDS length	452	321
Median intron length	2,227	3,046
Median exon number	4	3
Percentage of genome covered by genes	26.64	25.85

Table 1. The Statistics of Protein-Coding Genes in Payzawat and DHL92

A total of 1,761,822 SNPs and 735,486 indels were identified in syntenic blocks between the two genomes, respectively. Among them, 421,364 SNPs were located in the genic region (9,795 genes) and 33,636 in coding regions (6,971 genes) and 172,760 indels were located in the genic region (9,777 genes) and 4,548 in the coding region (1,842 genes) (Table S24, Figure 3A). For the SNPs within the coding regions, 3,128 SNPs (affecting796 genes) were non-synonymous or lead to changes at the start or stop codon. These genes were enriched in regulating fruit flavor (diterpenoid biosynthesis and the sulfur relay system) and cell wall biosynthesis (glycosylphosphatidylinositol [GPI]-anchor biosynthesis). The ratio of triple indels on the coding regions is higher than that on the non-coding regions (Figure 3B). The counts of SNPs and indels are higher on chr04, chr07, chr08, chr09, and chr12 (see Figure 3A). Genes with indels causing frameshift were mainly enriched in pathways relating to the cell wall (xylem development, glucuronoxylan metabolic process, xylan biosynthetic process, and D-xylose transport), flavor (organic substance transport and vacuolar transport), sugar metabolism (galactose transport, mannitol transport, sorbitol transport, and galactose transmembrane transporter activity), and fruit color (naringenin 3-dioxygenase activity). Some 49,394 structural variations, including GAP, JMP, INV, and SEQ, were detected on 5,852 genes (see Tables S25 and S26). In addition, 6,955 structural variations were detected in one-to-one syntenic blocks and 1,186 genes were affected. Among the genes located in syntenic blocks, approximately 5,181genes (23.51%, 22,037 in pseudochromosomes) of Payzawat showed variations in coding regions.

The skin (epidermis) of DHL92 (genome version CM3.6.1) is thin, whereas that of Payzawat is thick (see Figures S7A and S7B). To reveal the candidate genes involved in skin thickness, we analyzed the epidermis thickness-related quantitative trait loci (QTLs) (Diaz et al., 2011) and genes harboring SNPs, indels, and structural variations within these regions. QTL *STHQF12.4*, controlling the skin thickness, is located at 23,803,761–26,907,220 of chr12, consisting of 455 genes. Six genes (*EVM0008156:* pectinesterase, *EVM0009214:* gibberellin 20 oxidase 1-B-like, *EVM0016862*: pectate lyase-like, *EVM0014824*: pectinesterase, *EVM0014071*: pectinesterase, and *EVM0004080*: gibberellin 20 oxidase 1-B-like) with structural variants (SVs) were implicated in cell wall biosynthesis (see Figure 3C). The insertion of 76 bp on exon1 of *EVM0014842* on DHL92 leads to the truncated protein, and the variation on a region encompassing the start codon of *EVM0014071* and *EVM0016862* disables the function of these genes on DHL92 (Figure 3D). The sequence alignment showed the difference between the two genomes (see Figure S9). The other three genes in these two genomes were highly divergent. The variation status of six genes was checked in 49 re-sequencing samples, and the group information is shown in Figure 4B. The ratios of genes with variation in the TC (thick epidermis) group (group three) were higher compared with the TN (thin epidermis) group, such as *EVM0008156*, *EVM0009214*, and *EVM0014824*, and some genes showed the contrary, such as *EVM0004080* and *EVM0014071*. Variation of *EVM0016862* only can be detected in R13 (African horned melon [*Cucumis metuliferus*]) (see Figure S10). The variants for *EVM0016862* between Payzawat and DHL92 may be not real due to the poor assembly quality of the gene. 15 samples downloaded from NCBI (see Table S29), consisting of thick- and thin-skinned melons, were used to test the expression of

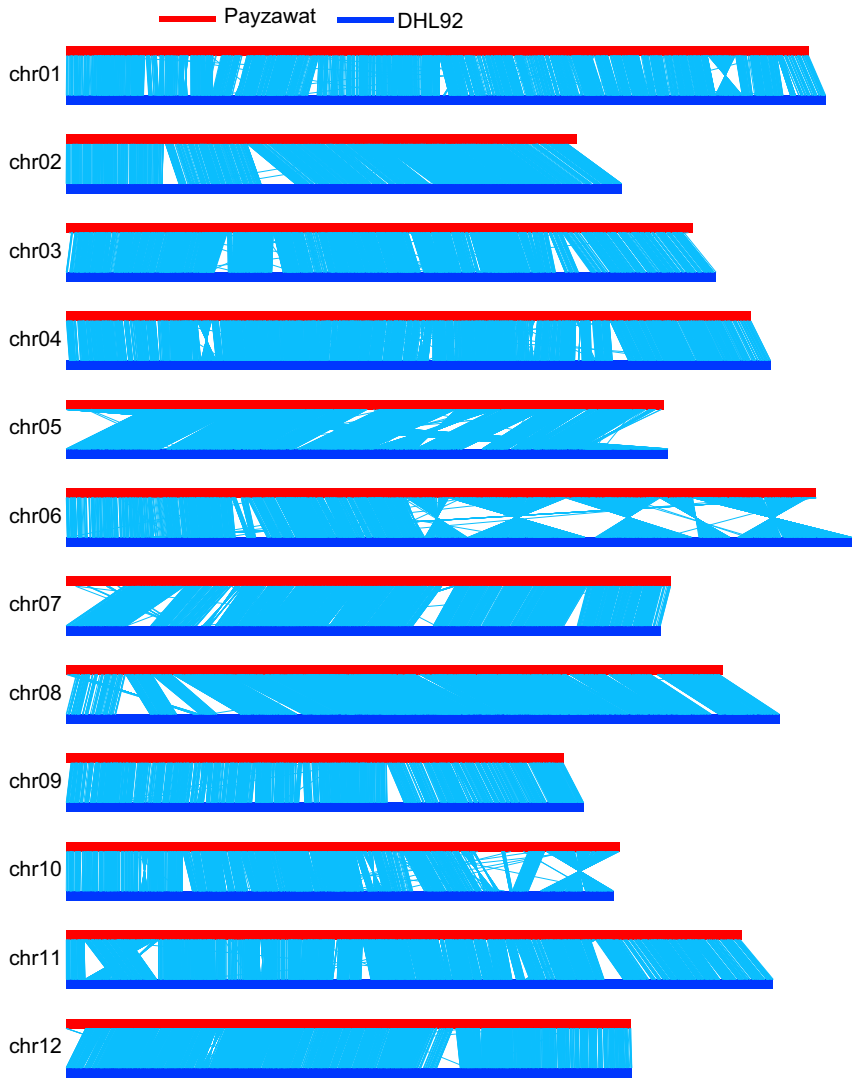

Figure 2. Whole Genome Alignment between Payzawat and CM3.6.1

The red bar represents the chromosome of Payzawat, and the deep navy-blue bar represents the chromosome of CM3.6.1. The sky blue line indicates synteny between Payzawat and CM3.6.1.

six genes. Except for one gene, which did not express at any sample, other five genes expressed more or less in the thick-epidermis melon (see Figure S11). All the above-mentioned evidence indicates that the six genes may function in determining the thickness of the epidermis.

The chromosome-level genomes for Payzawat and CM3.6.1 enable the identification of large structural variations and complex genome rearrangement. Large structural variations between Payzawat and CM3.6.1 are intra-chromosomal translocation and inversion. To exclude the assembly error leading to these differences, PacBio sub-reads were mapped to the inversion breakpoints of five large inversions on chromosome 6 (see Tables S27 and S28 and Figure 2). All breakpoints were covered by PacBio sub-reads (see Figure S8), validating the quality of Payzawat assembly. The structure of Payzawat chromosome 6 is also supported by Hi-C contact frequency heatmapping. This discrepancy may be the true difference between the two lines or the erroneous assembly of CM3.6.1 in this region. Some QTLs, *EayQL6.1* for early yield, *FDQN6.1* for fruit diameter, *PHYQN6.2* for phytoene content, *β-carQN6.1* for α-carotene content, and *fwi6.1* for fruit width (Diaz et al., 2011), were found to be co-located within the inversion regions on chromosome 6.

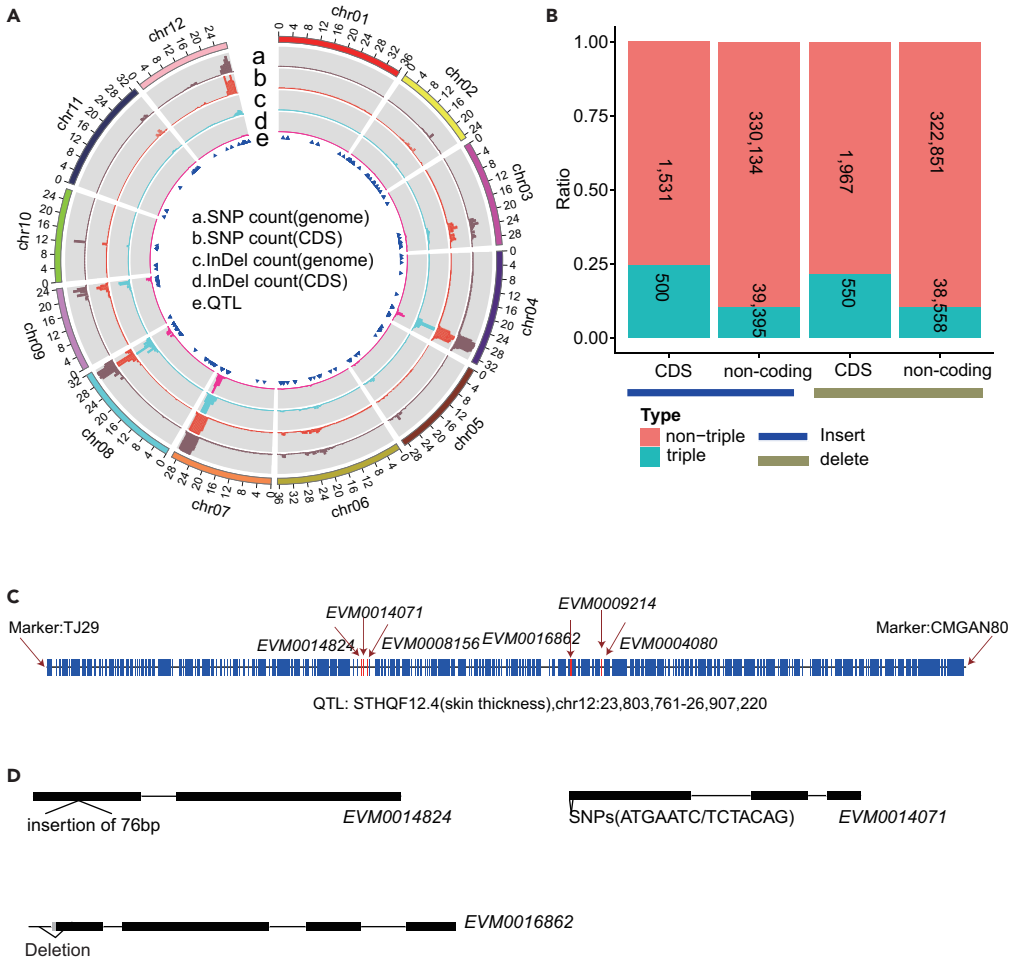

Figure 3. Genome-Wide Comparison between Payzawat and DHL92

(A) Distribution of SNP and indel count on the genome and coding regions at 100-Kb interval and the distribution of QTLs.

(B)The bar plot of triple and non-triple indels on genomic and coding regions.

(C) QTL STHQF12.4 regions on chromosome 12. Each blue line indicates one gene.

(D)The mutation of gene on DHL92 compared with Payzawat.

Payzawat is characterized as large fruit size, sweetness, and orange fleshy pulp, whereas DHL92 is medium fruit size and white fleshy pulp (see Figures S7A and S7B). Comparative genomic analysis uncovers numerous line-specific variations, which may serve as the important resource for such trait differences.

Genome Resequencing and Population Analysis

Resequencing of the 50 melon accessions (Figure 4A) generated a total of clean 90,443,068 paired-end (PE) reads, with an average of 18X depth per accession (Tables S30 and S31), and the mapping rate ranged from 86.74% to 95.63% when R13 is excluded owing to its distantly phylogenetic relationship with species *melo* (see Tables S31 and S32).

A total of 240,775 (4.65%; 5,174,489 in total) and 12,794 indels (0.97%; 1,316,073 in total) were located in coding sequences (CDS), among which 98,701 SNPs were non-synonymous and 6,453 indels led to frameshift mutations.

Neighbor-joining phylogenetic tree recovered from 50 melon accessions showed two clades (see Figure 4B). The sub-species agrestis did not cluster into one clade. Cultivars/landraces and the wild accessions of northern and southern China in sub-species agrestis formed a subclade and then grouped with the

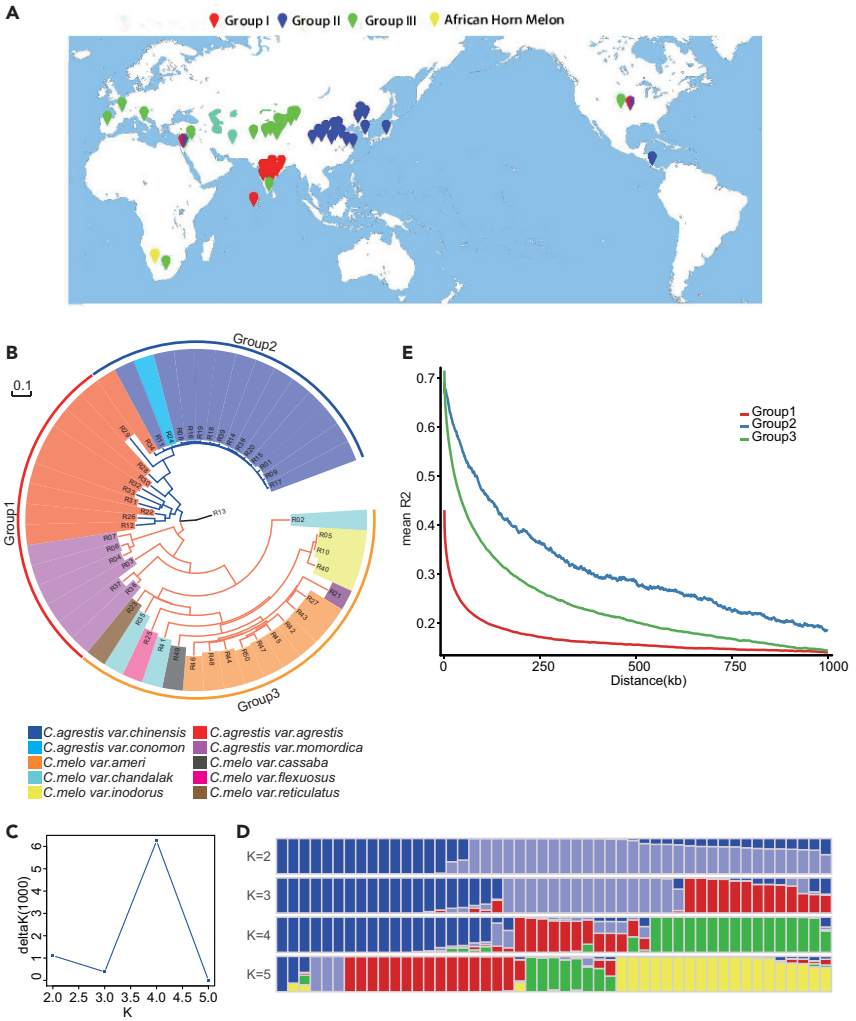

Figure 4. Population Structure Analysis

(A) The geographical distribution of resequencing samples.

(B) Neighbor-joining phylogenetic tree of the 50 melon accessions.

(C) K value estimation.

(D) Population structure of 49 resequencing accessions estimated by ADMISTURE. Each color indicates one ancestral population. Each bar indicates one accession.

(E) Decay of linkage disequilibrium for wild melon, subclade two and subclade four.

Indian wild subclade, indicating China may be one Asian diversifying center, supporting the idea that some oriental Asian melons originated from India, then spread into northern and southern China before domestication (Akashi et al., 2002; Yashiro et al., 2005). The cultivars/landraces on sub-species agrestis was designated as Group two, with a characteristic thin epidermis (TN group) (see Figure S7D).

The cultivars/landraces on sub-species melo, designated as Group three, have the characteristic of a thick epidermis (TC group) (see Figure S7B), with different geographical origins first grouped together and then grouped with the Indian wild subclade, which supported the opinion that cultivars/landraces were introduced to western China via the Silk Road (Kitamura, 1951) after the domestication occurred in India. The wild melons on these two clades were designated as Group one. The fruit of wild-type (WT) is small compared with that of cultivar (CV) (see Figure S7C).

The evolutionary history of melons in China was further explored with Delta K (individual ancestry coefficients) values. Results revealed that four populations (K = 4) represent the best model (see Figure 4C)

and new sub-populations arose from each clade with K from 2 to 4 (see Figure 4D). When K was set to 4, new sub-populations arose from the wild species, indicating their high diversity and distinct phylogenetic relationships with domesticated melons. The cultivars/landraces were segregated into two sub-populations revealing the geographical distributions thereof in China.

Together, these findings led us to propose the melon evolutionary history in China, revealing that China may be one of the diversifying centers and illustrating the idea that melons in different regions of China originated from distinct Indian regions and spread into China via multiple routes.

Population genetic analysis among groups was performed to test whether, or not, China was a diversification center. Nucleotide diversity (π) and Tajima's D were highest in the WT group (π = 0.0020285 and Tajima's D = 1.59854), followed by Group three (TC group, π = 0.0011642 and Tajima's D = 0.87328), and lowest in Group two (TN group, π = 0.0002681and Tajima's D = −0.50861), indicating the higher diversification of melons in northern and southern China (Group two).

LD analysis further confirmed the nucleotide diversity results. Linkage disequilibrium (LD) analysis for Group two (mainly containing melons from northern and southern China) has a much slower decay of pairwise correlation (r^2) values than for Group three (melons from western China) (see Figure 4E). Population analysis indicates that northern and southern China may be one of the diversification centers.

Selective Sweep Analysis

The fixation index (Fst) and π were used to detect the sweep signals between the wild (Group1) and cultivated (Groups 2 and 3) populations (see Figure 5A). Some 42,311,973-bp segments were recognized as sweep regions. Since the contrasting genotypes between wild and cultivated populations may contribute to the different phenotypes, e.g., fruit size, leaf size, seed size, and bitterness of the fruit, we focus on those genes with different genotypes between the wild and cultivated populations within the sweep regions. Among 26,919 small mutations (21,010 SNPs and 5,909 indels), 275 mutations (194 genes) change across the coding regions (non-synonymous mutation, start gained, stop gained, coding region change, insertion, deletion, and stop loss), providing the candidate pool for fruit trait improvement (Table S34). These genes were implicated in processes relating to fruit size (expansin-A12, cell division, and cell cycle), fruit development (brassinosteroid biosynthesis, the ethylene-activated signaling pathway, indole-3-acetic acid-induced protein ARG7, etc.), synthesis and transport of sugar (beta-glucosidase and alpha-L-fucosidase 2), fruit flavor (organic substance metabolism, carotenoid cleavage dioxygenase, water transport, solute carrier family, etc.), and biotic or abiotic response (disease resistance protein, etc.) (see Table S34).

CmACS7 is involved in sex determination, and a causal SNP was reported to be associated with andromonoecy. *CmACS7* affected fruit size through the SNP (C_small fruit-T_large fruit) regulating andromonoecy (Boualem et al., 2008). The gene was co-located with the selective sweep regions. The SNP at A57V (chr01:35853579:C-T) is linked with andromonoecy (see Figure 5B). Interestingly, most wild accessions had the same haplotype as the V57 mutant (andromonoecious), whereas the allele of cultivars/landraces equals *CmACS7* (monoecious) (see Figure 5C and Table S34). The gene *CmACS7* was also implicated in fruit weight, total soluble solids, and ethylene contents (Galpaz et al., 2018).Except for *CmACS7*, the other six genes, including *EVM0005618* (3-epi-6-deoxocathasterone 23-monooxygenase), *EVM0005054* (mitotic B-type cyclin), *EVM0010492* (VAL2), *EVM0018337* (cyclin-B3-1), *EVM0010058* (CCD1, carotenoid 9,10 (9′,10′)-cleavage dioxygenase 1), and *EVM0009845* (early flowering 3, ELF3) were involved in fruit development, leaf and seed development, and regulation of flower development and flowering. The SNP leading to non-synonymous mutations on these genes may contribute to the difference in fruit size, leaf size, and seed size between WT and CV populations (Figure 5B). The differentiated haplotypes of these SNPs for WT (group one) and CV (group two and group three) could be detected (see Figure 5C). Heterogeneity of the genotype in the wild or CV populations may be due to the complicated taxonomic history of melon, leading to a high number of misclassified germplasm collections. The variations on these genes may be involved in the fruit, seed, or leaf size, and more dense sampling, especially for wild populations, is necessary.

Identification of Candidate Haplotypes for Reported Genes

The resequencing data can also be used to identify and validate the candidate causal mutation for previously reported genes. We focus on small mutation on the coding regions (non-synonymous mutation, start gained, stop gained, coding region change, insertion, deletion, and stop loss).

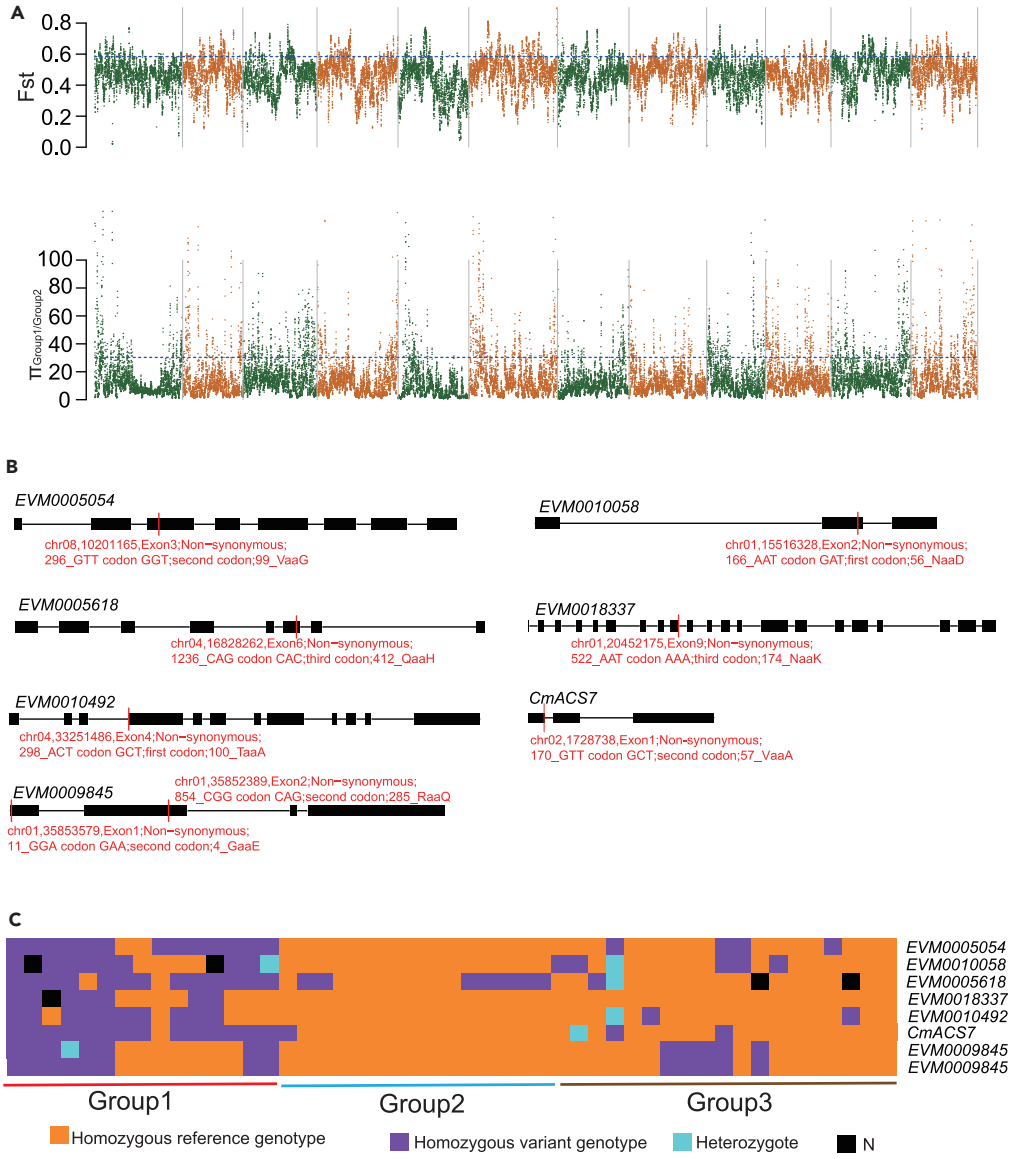

Figure 5. Candidate Alleles for Domestication Traits

(A) The upper panel is Fst for 100-kb windows compared between group one and group two. The bottom panel is π for 100-kb window compared between group one and group two.

(B) The structures of candidate genes implicated in domestication traits and the positions of the mutations on the gene. The black rectangles represent coding sequences (CDS) and the black lines between rectangles are introns. The red line on the CDS indicates the position of causative SNP/InDel.

(C) Haplotype distributions for these genes according to different groups.

The *pH* gene has a significant effect on fruit acidity via a 12-base duplication on coding region, and most sweet melons have this duplication (Cohen et al., 2014). *pH* in Payzawat matched the allele of sweet melon, with 12-bp (TTAATTGTTGCA) duplication in the coding region, whereas the allele in DHL92 matched the allele of sour melon. Wild accessions matched the allele of sour melon, whereas cultivars/landraces accessions matched both alleles (see Figure S12 and Table S34), indicating that acidity is the diversifying trait (see Figure S12).

CmOr gene was the causal gene for difference of orange and non-orange colors (Tzuri et al., 2015), and a single SNP (G_green flesh->A_orange flesh) is responsible for the different flesh color pigmentation. The

allele in Payzawat matched the allele of orange melon (''Dulce''), whereas the allele in CM3.6.1 matched the allele of non-orange melon (''Tam Dew''). Sub-species agrestis (Group one and Group two) accessions matched the allele of non-orange melon, whereas sub-species melo (Group three) accessions matched the allele of orange melon (see Table S34 and Figure S12), indicating that the flesh color is the diversifying, or selection, trait.

ETHQB6.3 controls fruit ripening type (climacteric and non-climacteric), and *MELO3C016540* was recognized as the causal gene (Ríos et al., 2017). We detected one SNP on *EVM0015173*, homologous to *MELO3C016540*. CmKFB (*EVM0012228*) is implicated in the accumulation of naringenin chalcone, which determined the yellow color of rind (Feder et al., 2015).

Candidate genes *EVM0015625* and *EVM0019658* were on the QTL SUCQSC5.1, which is responsible for sugar accumulation (Argyris et al., 2017). *CmTHAT1* (acetyl-CoA acetyltransferase, *EVM0016460*) affects fruit flavor. *CmPPR1* (pentatricopeptide repeat-containing protein, *EVM0014144*) genes may affect carotenoid accumulation and flesh color, which may correspond to the *wf* locus (Galpaz et al., 2018). *RGH10* (*EVM0014144*) confers resistance to Papaya ring-spot virus (PRSV) and *RGH9* (*EVM0004621*) confers resistance to races 0 and 2 (Brotman et al., 2013). *ACS11* (*EVM0021716*) is involved in sex determination (Boualem et al., 2015), and some contrasting haplotypes were detected in TC and TN groups, such as SUCQSC5.1, *CmTHAT1*, and *RGH10*; some were detected in sub-species agrestis and melo, such as *RGH9*, *PPR1*, and ETHQB6.3. These traits are diversifying and showed taxonomic specificity.

The population analysis provides the basis of genetic control of many traits, e.g., flowering, fruit morphology, ripening behavior, rind characteristics, flesh color, and sugar content. The results will expand our knowledge of candidate genes controlling desirable traits.

DISCUSSION

In summary, by combing the SMRT sequencing technology and high-throughput chromosome interaction mapping technology, we obtained a high-quality melon genome with contig N50 up to 2.8 Mb and more than 98.53% sequences were anchored to 12 chromosomes, which provided a fine genome for future melon studies. Compared with use of NGS technology, SMRT sequencing exhibited superiority in genome assembly. Compared with traditional genetic maps, Hi-C technology exhibits several advantages in chromosome construction, such as encompassing up to one million markers, being convenient when preparing materials and offering high accuracy at lower cost. Both technologies help us obtain more intact genome information, which should be helpful in understanding the genetic changes in long-term natural evolution and artificial domestication of melon.

A high-quality genome assembly with higher contiguity and completeness shows its values in studying evolution, domestication, and breeding, as well as gaining insights into genome-wide structural variants (Sun et al., 2018; Zhang et al., 2019; Xie et al., 2019). The whole-genome sequence comparison between Payzawat and DHL92 enables the identification of the large inversions, e.g., five inversions on the tail of chromosome 6, and translocations, e.g., translocation on chromosome 5. These differences between two genomes may be line-specific or mis-assembly, and further validation of assembly quality is necessary. The comparative genomic analysis between Payzawat and DHL92 indicates that chromosome regions (e.g., Chr3, Chr4, Chr7, Chr8, Chr9, and Chr12) enriched with small variations (SNP and InDels) tend to colocalize with QTLs. The QTL STHQF12.4 (skin thickness) was located on chr12 (23,803,761–26,907,220), where small variations were enriched. Six genes annotated with pectinesterase, gibberellin 20 oxidase 1-B-like, and pectate lyase-like, and these six genes have variations in resequencing data. The homologs of pectinesterase, gibberellin 20 oxidase 1-B-like, and pectate lyase-like in plants are involved in cell wall biosynthesis (Micheli, 2001; Alqsous et al., 2004; Yang et al., 2017; Jeon; et al., 2016; Bai et al., 2014). The correlation between expression profiles of six genes and epidermis thickness must be tested in more samples. There is a shortage in the number of samples in our present analysis, and whether the six genes have variants in samples should be checked. Owing to the unavailable data (transcriptome data and resequencing data for each sample), the conclusion is less strong at present. More samples should be included in future to test the correlation among expression profiles, structural variants, and skin thickness. The identification of variants (large structural variants and small variants) will

allow the exploration of genotypes and phenotypes. However, the mechanism controlling the skin thickness in melon remains to be explored.

Previously, evidence backing up multiple domestications in melon was mostly derived from short DNA sequences (Endl et al., 2018), and whole-genome level evidence is more persuasive. We here present evidence supporting multiple domestications in melon from the whole-genome perspective. Because most samples in our study were collected from China, more samples from wider geographical locations are needed to strengthen the evidence. The higher diversification in northern and southern melons (TC group) compared with the western melons (TN group) supported with LD, π, and Tajima's D explains the diverse shape, color, etc. in the TC group. The haplotype analysis indicates that some traits in modern melons, like fruit size through evaluating the haplotype of causative SNP in CmACS7, are domesticated from wild melon and some traits are lineage specific. The domestication and diversification processes contribute to the breeding through providing the molecular foundation.

Limitations of the Study

We reported a high-quality assembly of melon. We identified six genes potentially related to skin thickness. More samples are required to test the correlation among the variation, expression profile of six genes, and skin thickness. Furthermore, the samples for population analysis are inadequate and samples from wider geographical locations are needed.

METHODS

All methods can be found in the accompanying Transparent Methods supplemental file.

DATA AND CODE AVAILABILITY

The DNA short reads, RNA-seq data, linked reads, and Pacbio sub-reads used in this study were submitted to NCBI under submission number SUB4523929 and project number PRJNA491307. The accession number for Payzawat genome assembly reported in this paper is SUB6534844 under the project PRJNA491307. The resequencing raw data have been deposited into NCBI Short Read Archive with the accession number SRP081058.

SUPPLEMENTAL INFORMATION

Supplemental Information can be found online at https://doi.org/10.1016/j.isci.2019.10.049.

ACKNOWLEDGMENTS

This study was supported by The National Natural Science Foundation of China (Grant No. 31860564, http://www.nsfc.gov.cn), the Special Fund for Agroscientific Research in the Public Interest of The Ministry of Agriculture of the People's Republic of China (Grant No. 201203004), and the earmarked fund for Modern Agro-industry Technology Research System (Grant No. CARS-25).We would like to thank Jordi Garcia-Mas from Centre de Recerca en Agrigenòmica CSIC-IRTA-UAB-UB, Campus UAB, Edifici CRAG for providing the picture and trait information of DHL92 in this paper.

AUTHOR CONTRIBUTIONS

Conceptualization, H. Yi, H. Zhang, and H. Zheng; Methodology, X. Li, H. Yu, M. Liu, C. Ji, L. Ma, J. Tang, and J. Miao; Investigation, H. Zhang, Y. Zhang, M. Li, Ha. Wang, D. Wang, Hu. Wang, and Q. Fu; Visualization, H. Yu, L. Ma, and J. Tang; Writing – Original Draft, H. Zhang, H. Yi, X.Li, and H. Yu; Writing – Review & Editing, H. Zhang, and H. Yu; Supervision, H. Yi.

DECLARATION OF INTERESTS

The authors declare no competing interests.

Received: July 24, 2019
Revised: September 23, 2019
Accepted: October 24, 2019
Published: December 20, 2019

REFERENCES

Akashi, Y., Fukuda, N., Wako, T., Masuda, M., and Kato, K. (2002). Genetic variation and phylogenetic relationships in East and South Asian melons, *Cucumis melo* L. based on the analysis of five isozymes. Euphytica *125*, 385–396.

Akdemir, K.C., and Chin, L. (2015). HiCPlotter integrates genomic data with interaction matrices. Genome Biol. *16*, 198.

Alqsous, S., Carpentier, E., Kleineude, D., Burel, C., Mareck, A., Dauchel, H., Gomord, V., and Balangé, A.P. (2004). Identification and isolation of a pectin methylesterase isoform that could be involved in flax cell wall stiffening. Planta *219*, 369–378.

Argyris, J.M., Ruiz-Herrera, A., Madriz-Masis, P., Sanseverino, W., Morata, J., Pujol, M., Ramos-Onsins, S.E., and Garcia-Mas, J. (2015). Use of targeted SNP selection for an improved anchoring of the melon (*Cucumis melo* L.) scaffold genome assembly. BMC Genomics *16*, 4.

Argyris, J.M., Díaz, A., Ruggieri, V., Fernández, M., Jahrmann, T., Gibon, Y., Picó, B., Martín-Hernández, A.M., Monforte, A.J., and Garcia-Mas, J. (2017). QTL analyses in multiple populations employed for the fine mapping and identification of candidate genes at a locus affecting sugar accumulation in melon (*Cucumis melo* L.). Front. Plant Sci. *8*, 1679.

Bai, W., Xiao, Y., Zhao, J., Song, S.Q., Hu, L., Zeng, J.Y., Li, X.B., Hou, L., Luo, M., Li, D.M., and Pei, Y. (2014). Gibberellin overproduction promotes sucrose synthase expression and secondary cell wall deposition in cotton fibers. PLoS One *9*, e96537.

Bickhart, D.M., Rosen, B.D., Koren, S., Sayre, B.L., Hastie, A.R., Chan, S., Lee, J., Lam, E.T., Liachko, I., Sullivan, S.T., et al. (2017). Single-molecule sequencing and chromatin conformation capture enable de novo reference assembly of the domestic goat genome. Nat. Genet. *49*, 643–650.

Boualem, A., Fergany, M., Fernandez, R., Troadec, C., Martin, A., Morin, H., Sari, M.A., Collin, F., Flowers, J.M., Pitrat, M., et al. (2008). A conserved mutation in an ethylene biosynthesis enzyme leads to andromonoecy in melons. Science *321*, 836–838.

Boualem, A., Troadec, C., Céline, C., Lemhemdi, A., Morin, H., Sari, M.A., Fraenkel-Zagouri, R., Kovalski, I., Dogimont, C., Perl-Treves, R., and Bendahmane, A. (2015). A cucurbit androecy gene reveals how unisexual flowers develop and dioecy emerges. Science *350*, 688–691.

Brotman, Y., Normantovich, M., Goldenberg, Z., Zvirin, Z., Kovalski, I., Stovbun, N., Doniger, T., Bolger, A.M., Troadec, C., Bendahmane, A., et al. (2013). Dual resistance of melon to *Fusarium oxysporum* races 0 and 2 and to papaya ring-spot virus is controlled by a pair of head-to-head-oriented NB-LRR genes of unusual architecture. Mol. Plant *6*, 235–238.

Cohen, S., Itkin, M., Yeselson, Y., Tzuri, G., Portnoy, V., Harel-Baja, R., Lev, S., Sa'ar, U., Davidovitz-Rikanati, R., Baranes, N., et al. (2014). The PH gene determines fruit acidity and contributes to the evolution of sweet melons. Nat. Commun. *5*, 4026.

Diaz, A., Fergany, M., Formisano, G., Ziarsolo, P., Blanca, J., Fei, Z., Staub, J.E., Zalapa, J.E., Cuevas, H.E., Dace, G., et al. (2011). A consensus linkage map for molecular markers and Quantitative Trait Loci associated with economically important traits in melon (*Cucumis melo* L.). BMC Plant Biol. *11*, 111.

Diaz, A., Martinhernandez, A.M., Dolcetsanjuan, R., Garcesclaver, A., Alvarez, J.M., Garciamas, J., and Monforte, A.J. (2017). Quantitative trait loci analysis of melon (*Cucumis melo* L.) domestication-related traits. Theor. Appl. Genet. *130*, 1837–1856.

Endl, J., Achigandako, E.G., Pandey, A.K., Monforte, A.J., Pico, B., and Schaefer, H. (2018). Repeated domestication of melon (*Cucumis melo*) in Africa and Asia and a new close relative from India. Am. J. Bot. *105*, 1662–1671.

Feder, A., Burger, J., Gao, S., Lewinsohn, E., Katzir, N., Schaffer, A.A., Meir, A., Davidovich-Rikanati, R., Portnoy, V., Gal-On, A., et al. (2015). A Kelch domain-containing F-box coding gene negatively regulates flavonoid accumulation in *Cucumis melo* L. Plant Physiol. *169*, 1714–1726.

Galpaz, N., Gonda, I., Shem-Tov, D., Barad, O., Tzuri, G., Lev, S., Fei, Z., Xu, Y., Mao, L., Jiao, C., Harel-Beja, R., et al. (2018). Deciphering genetic factors that determine melon fruit-quality traits using RNA-seq-based high-resolution QTL and eQTL mapping. Plant J. *94*, 169–191.

Garcia-Mas, J., Benjak, A., Sanseverino, W., Bourgeois, M., Mir, G., González, V.M., Hénaff, E., Câmara, F., Cozzuto, L., Lowy, E., et al. (2012). The genome of melon (*Cucumis melo* L.). Proc. Natl. Acad. Sci. U S A *109*, 11872.

Gordon, D., Huddleston, J., Chaisson, M.J., Hill, C.M., Kronenberg, Z.N., Munson, K.M., Malig, M., Raja, A., Fiddes, I., Hillier, L.W., et al. (2016). Long-read sequence assembly of the gorilla genome. Science *352*, aae0344.

Jarvis, D.E., Ho, Y.S., Lightfoot, D.J., Schmockel, S.M., Li, B., Borm, T.J., Ohyanagi, H., Mineta, K., Michell, C.T., Saber, N., et al. (2017). The genome of *Chenopodium quinoa*. Nature *542*, 307–312.

Jeon, H.W., Cho, J.S., Park, E.J., Han, K.H., Choi, Y.I., and Ko, J.H. (2016). Developing xylem-preferential expression of PdGA20ox1, a gibberellin 20-oxidase 1 from *Pinus densiflora*, improves woody biomass production in a hybrid poplar. Plant Biotechnol. J. *14*, 1161–1170.

Kitamura, S. (1951). The origin of cultivated plants of China. Acta Phyotaxon. Geobot. *14*, 81–86.

Koren, S., Walenz, B.P., Berlin, K., Miller, J.R., Bergman, N.H., and Phillippy, A.M. (2017). Canu: scalable and accurate long-read assembly via adaptive k-mer weighting and repeat separation. Genome Res. *27*, 722–736.

Micheli, F. (2001). Pectin methylesterases: cell wall enzymes with important roles in plant physiology. Trends Plant Sci. *6*, 414–419.

Pitrat, M. (2013). Phenotypic diversity in wild and cultivated melons (*Cucumis melo*). Plant Biotechnol. *30*, 273–278.

Ríos, P., Argyris, J., Vegas, J., Leida, C., Kenigswald, M., Tzuri, G., Troadec, C., Bendahmane, A., Katzir, N., Picó, B., et al. (2017). ETHQV6.3 is involved in melon climacteric fruit ripening and is encoded by a NAC domain transcription factor. Plant J. *91*, 671–683.

Ruggieri, V., Alexiou, K.G., Morata, J., Argyris, J., Pujol, M., Yano, R., Nonaka, S., Ezura, H., Latrasse, D., Boualem, A., et al. (2018). An improved assembly and annotation of the melon (*Cucumis melo* L.) reference genome. Sci. Rep. *8*, 8088.

Simao, F.A., Waterhouse, R.M., Ioannidis, P., Kriventseva, E.V., and Zdobnov, E.M. (2015). 1,440 BUSCO embryophyta subset of genes: assessing genome assembly and annotation completeness with single-copy orthologs. Bioinformatics *31*, 3210–3212.

Sun, S., Zhou, Y., Chen, J., Shi, J., Zhao, H., Zhao, H., Song, W., Zhang, M., Cui, Y., Dong, X., et al. (2018). Extensive intraspecific gene order and gene structural variations between Mo17 and other maize genomes. Nat. Genet. *50*, 1289–1295.

Tzuri, G., Zhou, X., Chayut, N., Yuan, H., Portnoy, V., Meir, A., Sa'ar, U., Baumkoler, F., Mazourek, M., Lewinsohn, E., et al. (2015). A 'golden' SNP in CmOr governs the fruit flesh color of melon (*Cucumis melo*). Plant J. Cell Mol. Biol. *82*, 267–279.

Wang, X., Xu, Y., Zhang, S., Cao, L., Huang, Y., Cheng, J., Wu, G., Tian, S., Chen, C., Liu, Y., et al. (2017). Genomic analyses of primitive, wild and cultivated citrus provide insights into asexual reproduction. Nat. Genet. *49*, 765–772.

Xie, M., Chung, C.Y., Li, M., Wong, F.L., Wang, X., Liu, A., Wang, Z., Leung, A.K., Wong, T.H., Tong, S.W., et al. (2019). A reference-grade wild soybean genome. Nat. Commun. *10*, 1–12.

Yang, L., Huang, W., Xiong, F., Xian, Z., Su, D., Ren, M., and Li, Z. (2017). Silencing of SlPL, which encodes a pectate lyase in tomato, confers enhanced fruit firmness, prolonged shelf-life and reduced susceptibility to grey mould. Plant Biotechnol. J. *15*, 1544–1555.

Yashiro, K., Iwata, H., Akashi, Y., Tomita, K., Kuzuya, M., Tsumura, Y., and Kato, K. (2005). Genetic relationship among East and South Asian melon (*Cucumis melo* L.) revealed by AFLP analysis. Breed. Sci. *55*, 197–206.

Ye, C., Hill, C.M., Wu, S., Ruan, J., and Ma, Z.S. (2016). DBG2OLC: efficient assembly of large genomes using long erroneous reads of the third generation sequencing technologies. Sci. Rep. *6*, 31900.

Zhang, L., Hu, J., Han, X., Gao, Y., Richards, C.M., Zhang, C., Tian, Y., Liu, G., Gul, H., et al. (2019). A high-quality apple genome assembly reveals the association of a retrotransposon and red fruit colour. Nat. Commun. *10*, 1494.

ISCI, Volume *22*

Supplemental Information

A High-Quality Melon Genome Assembly Provides Insights into Genetic Basis of Fruit Trait Improvement

Hong Zhang, Xuming Li, Haiyan Yu, Yongbing Zhang, Meihua Li, Haojie Wang, Dengming Wang, Huaisong Wang, Qiushi Fu, Min Liu, Changmian Ji, Liming Ma, Juan Tang, Song Li, Jianshun Miao, Hongkun Zheng, and Hongping Yi

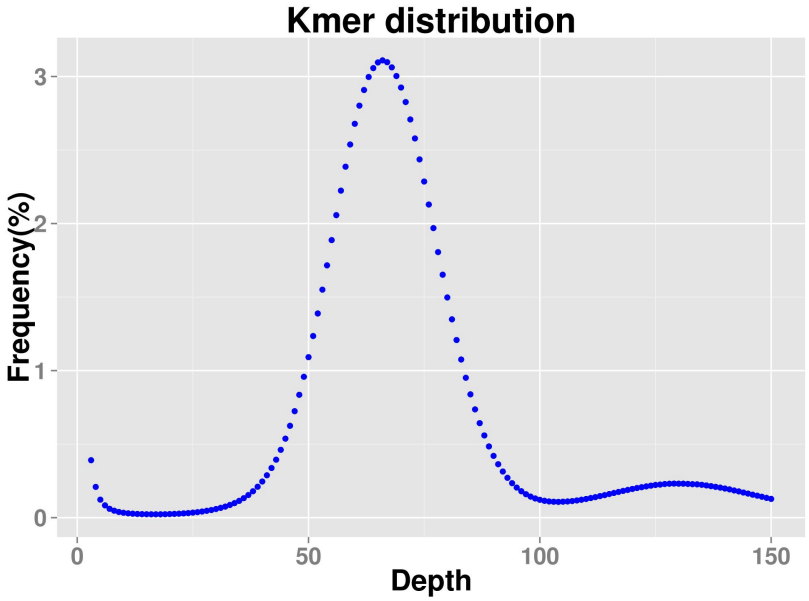

Figure S1. 17-Kmer frequency distribution using Illumina short reads. Related to Figure 1.

The depth of peak was at 64 and peak at depth of more than 128 was a repetitive peak.

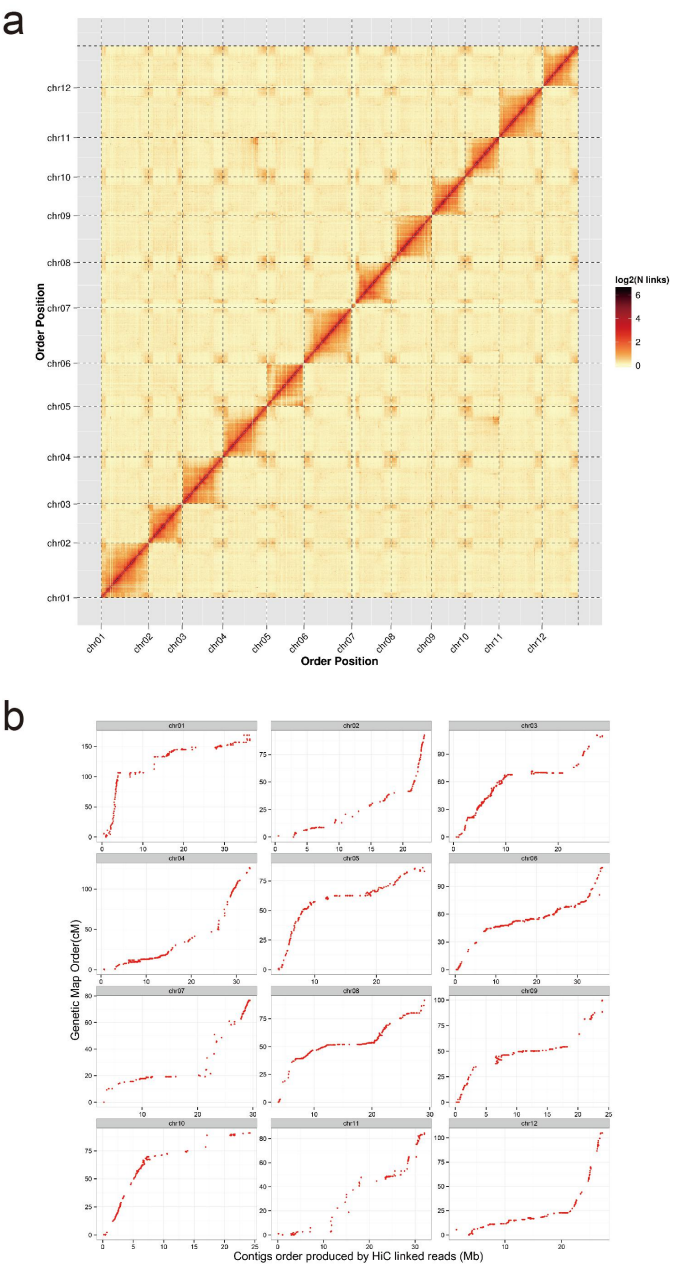

Figure S2. Assessment of genome assembly. Related to Figure 1.

a. The interaction frequency distribution of Hi-C links among Payzawat melon chromosomes. We scanned the genome using a 500-kb non-overlapping window as a bin and calculated valid interaction links of Hi-C data between any pair of bins. The base-2 logarithm of the link number was calculated. The distribution of links among chromosomes was exhibited by heat-map based on Hi-Cplotter. The colour key of the heat-map ranges from light yellow to dark red indicating the frequency of Hi-C interaction links from low to high (0 to 6).

b. The genetic-map-based evaluation of assembly. Genetic markers were mapped to the genome and locations were plotted according to the genetic map and HiC anchored pseudochromosomes.

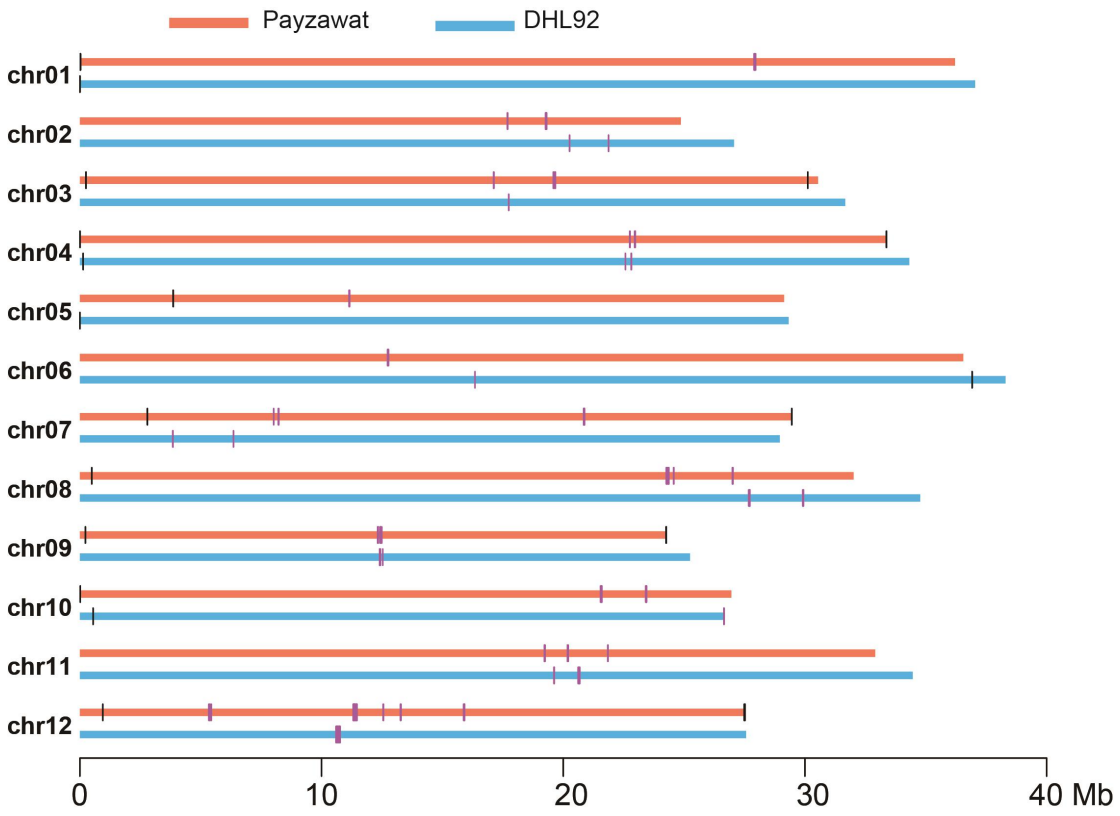

Figure S3. Identification of centromeric repeats and telomeric motifs on Payzawat assembly. **Related to Figure 1.** The red bar represents the chromosome of Payzawat and the blue bar represents the chromosome of CM3.6.1. The magenta rectangles indicate the position of centromeric repeats and the black rectangles indicates the position of telomeres.

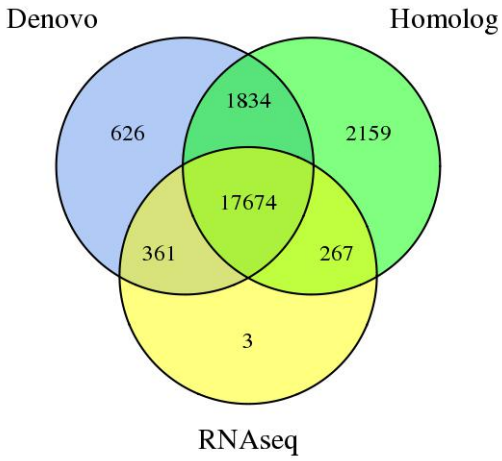

Figure S4. Veen plot of gene sets. **Related to Figure 1.**

The predicted genes were supported by *De novo*, homolog or transcriptome evidence.

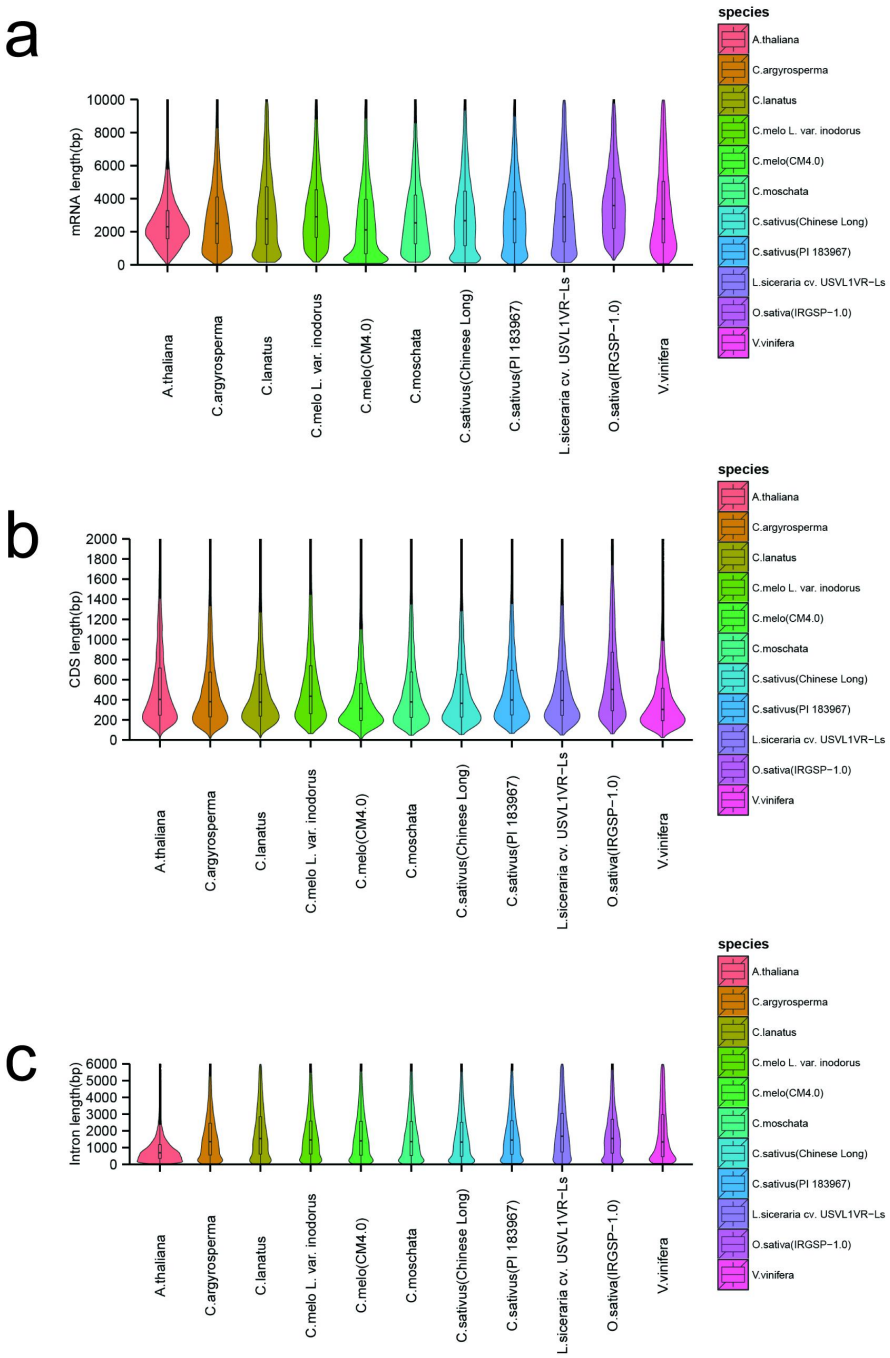

Figure S5. Length distribution of mRNA, CDS, and intron. Related to Figure 1.

a. Distribution of mRNA length in species within the Cucurbitaceae family and other plants; **b.** Distribution of CDS length in species within the Cucurbitaceae family and other plants; **c.** Distribution of intron length in species within the Cucurbitaceae family and other plants.

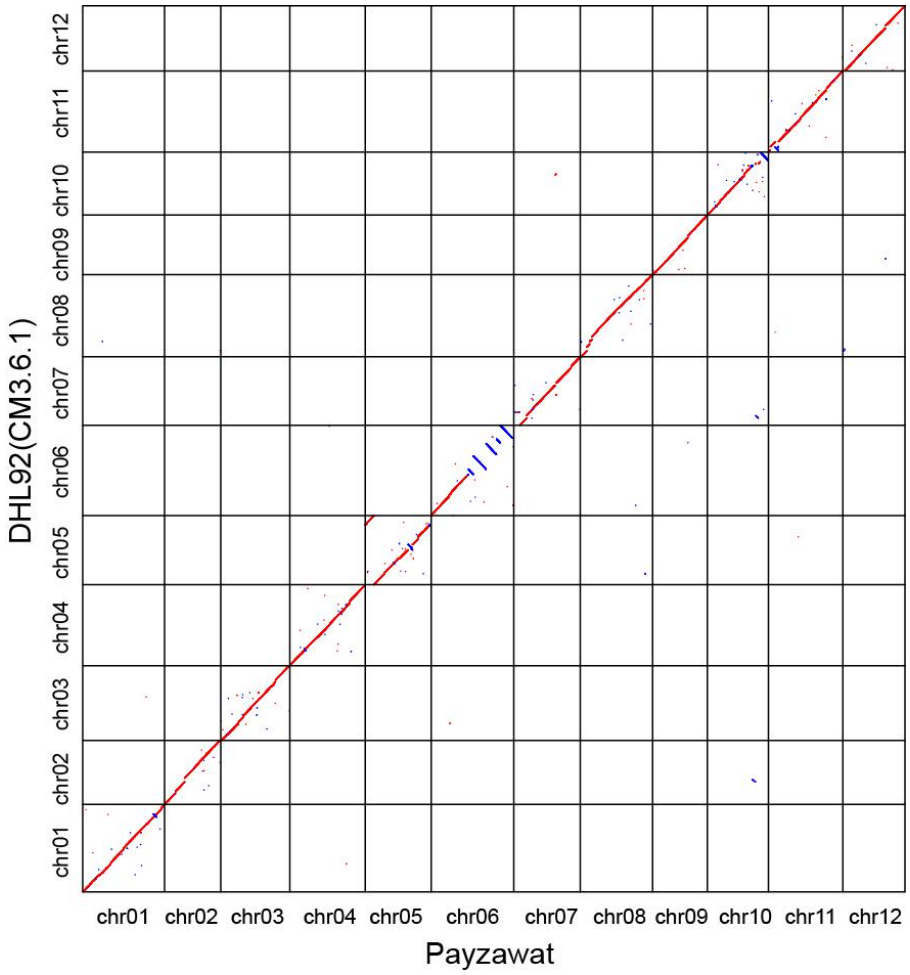

Figure S6. Whole genome comparison between Payzawat and CM3.6.1. Related to Figure 2.

The red line on the diagonal indicates the same orientation and the blue line indicates the reverse orientation.

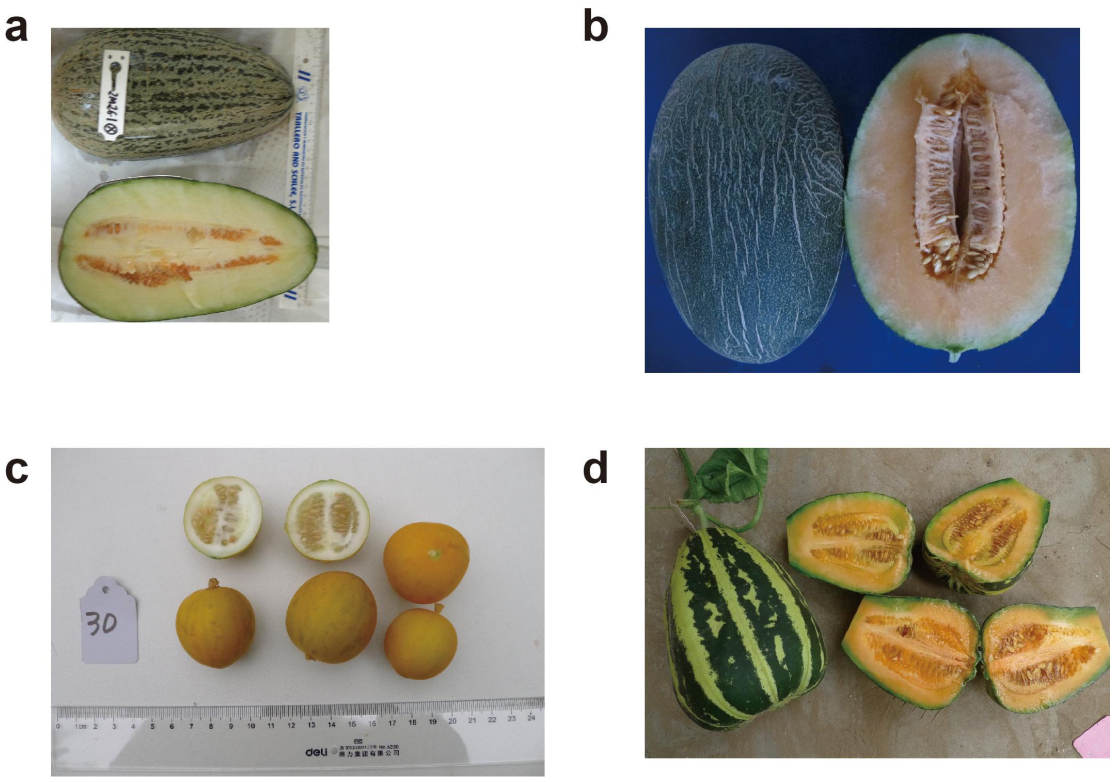

Figure S7. Fruit pictured: DHL92 (a), Payzawat (b), wild (c), and thin-skin melon (d). Related to Figure 2,3 and 4.

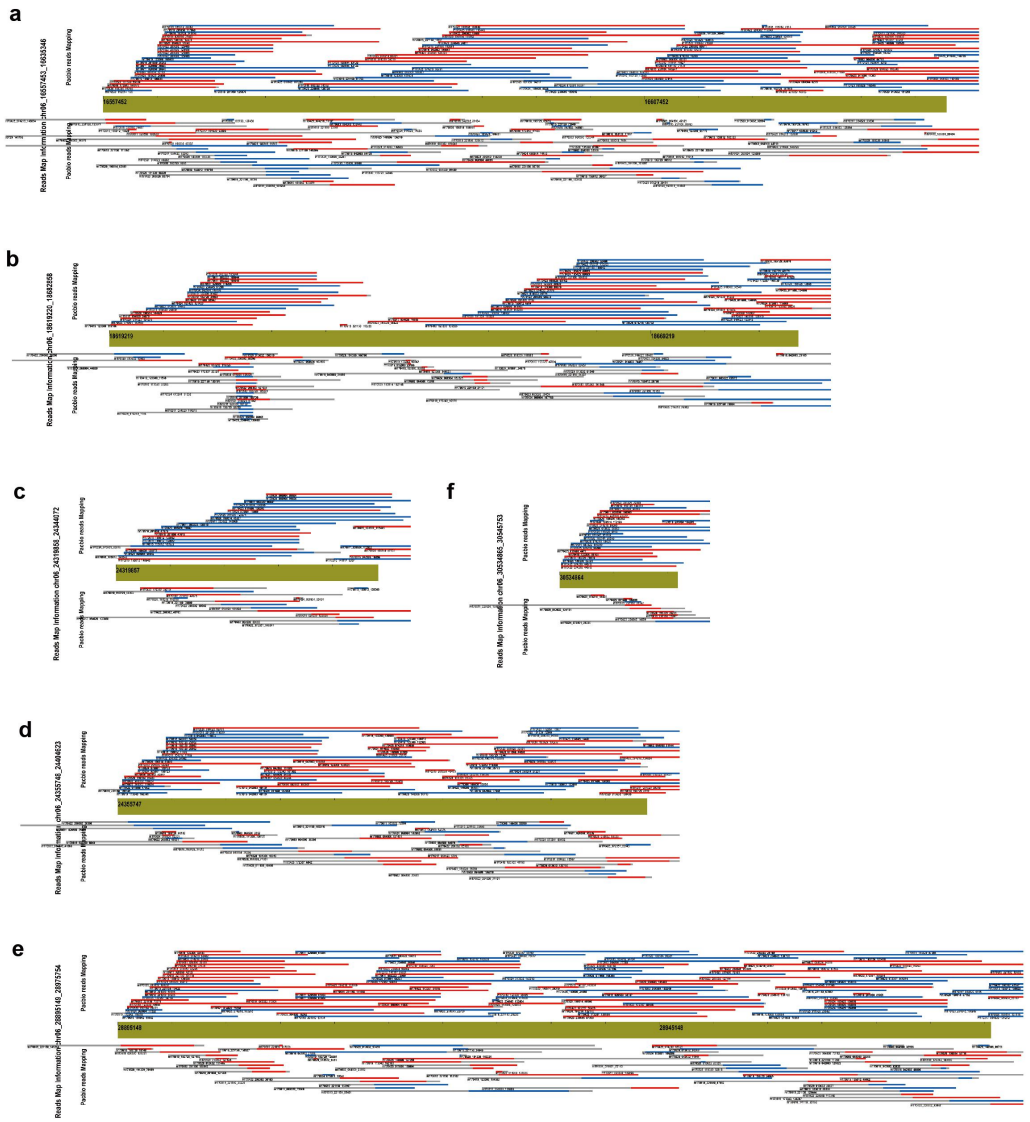

Figure S8. Validation of inversion breakpoints on chr06 through PacBio subreads mapping back to Payzawat assembly. **Related to Figure 2.**

a. PacBio subreads mapping to the left breakpoint of INV1. **b.** PacBio subreads mapping to the right breakpoint of INV1. **c.** PacBio subreads mapping to the right breakpoint of INV2. **d.** PacBio subreads mapping to the left breakpoint of INV3. **e**. PacBio subreads mapping to the right breakpoint of INV3. **f.** PacBio subreads mapping to the left breakpoint of INV5.

The red line indicates PacBio subreads mapping back to the Payzawat assembly on the forward orientation and the blue line indicates PacBio subreads mapping back to the Payzawat assembly on the reverse orientation. The grey line indicates non-mapping PacBio subreads. The green bar represents the segments of Payzawat assembly. The upper panel on the bar represents the high-quality mapping subreads and the lower panel on the bar represents

low-quality mapping subreads.

Figure S9. Sequence alignment for candidate genes implicated in skin thickness. Related to Figure 3.

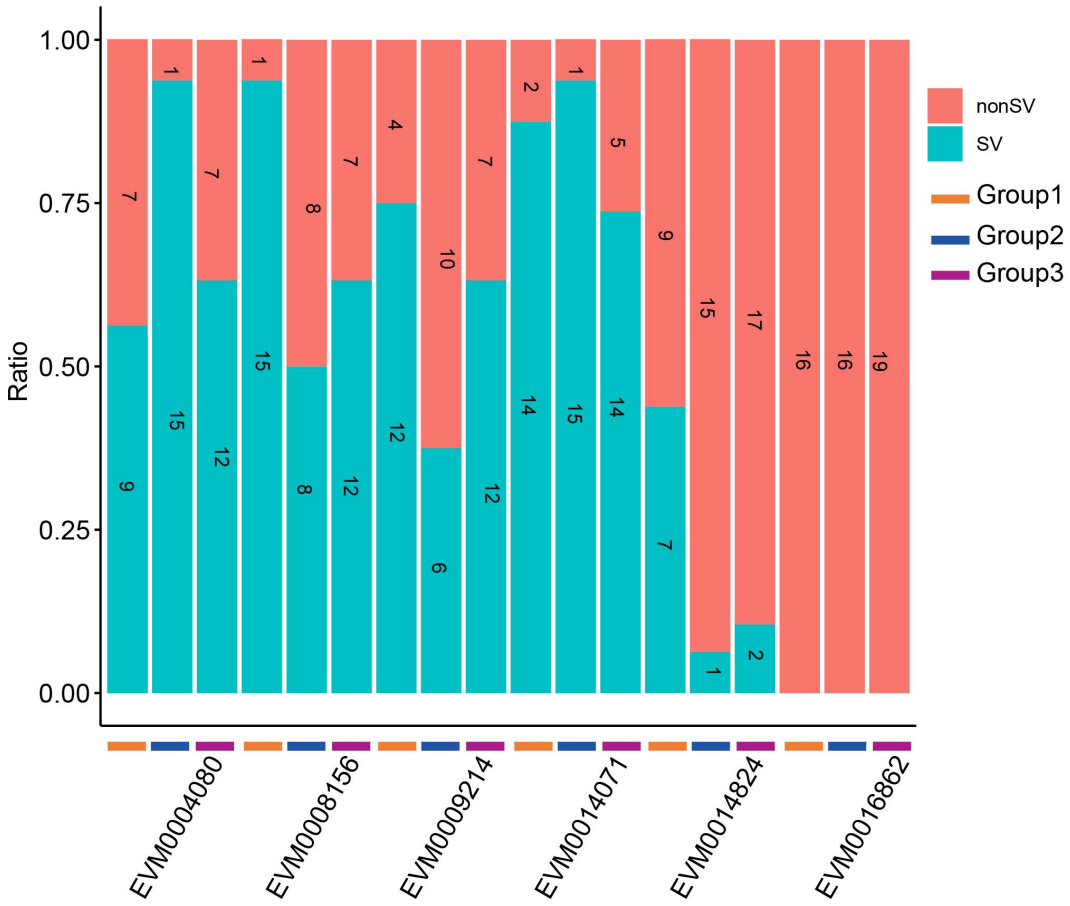

Figure S10. Variation of six genes in 49 resequencing samples. Related to Figure 3.

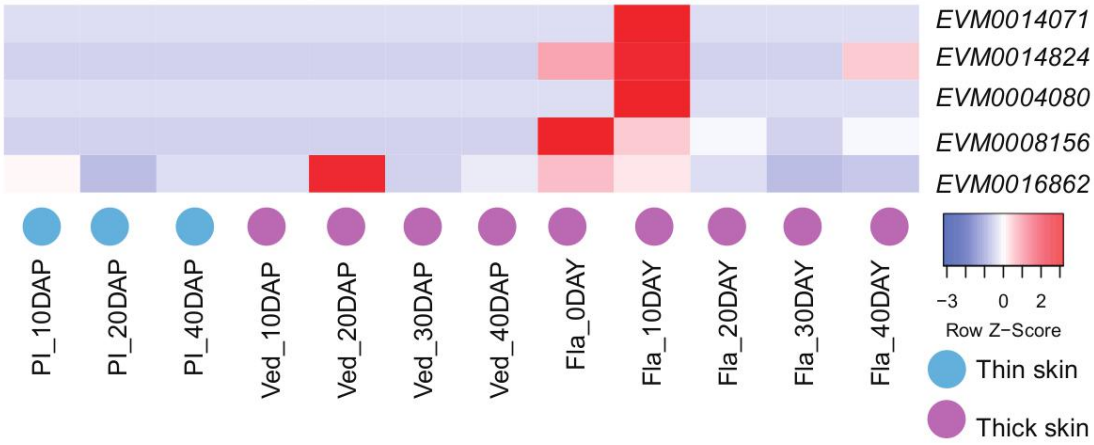

Figure S11. Expression profile of genes. Related to Figure 3.

DAP : day after pollination. PI: PI 161375 (PI, conomon group); Ved: cv. Védrantais (Ved; cantalupensis group); Fla:C. melo var ameri, cv 'Flavor No. 4'.

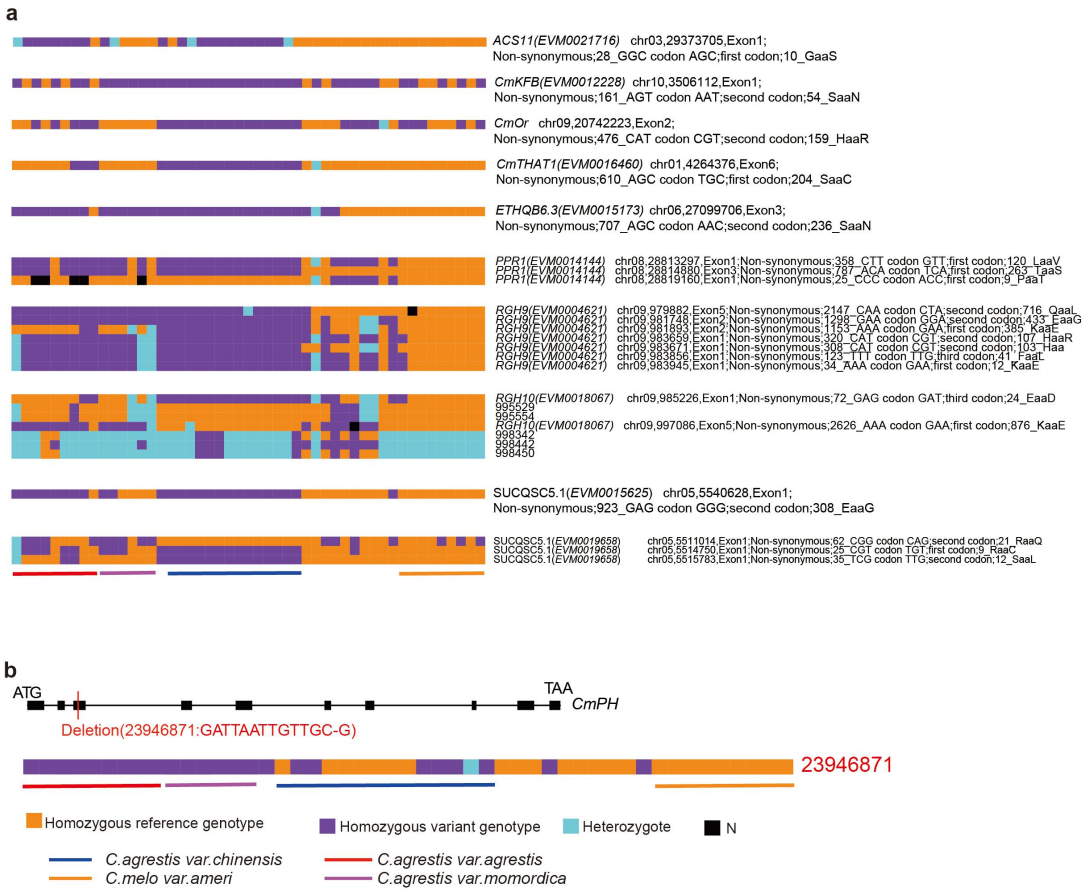

Figure S12. Candidate alleles for reported genes. Related to Figure 5.

a. candidate causative SNPs for reported genes. **b.** Structure and validated deletions for CmPH.

Table S1. Summary of Illumina PE reads for melon. Related to Figure 1.

Date type	Library Insert Size (bp)	PE Reads Number	Base Number	Q30
Genome survey and genome base error correction	270	108,577,515	32,528,871,468	91.94%
HiC data for genome error correction and chromosome construction	300~700	164,495,209	49,070,802,940	90.24%

Table S2a. Summary of SMRT reads for melon. Related to Figure 1.

Type	Filter	Read Bases (bp)	Reads Num	Read N50	Mean Reads Length (bp)	Reads Quality
Polymerase Reads	Pre-Filter	30,783,578,459	4,057,884	20,305	7,586	0.405
	Post-Filter	27,848,664,023	1,876,049	20,690	14,844	0.835
Subreads	Filter 500 bp	27,795,975,505	2,643,196	13,947	10,516	---

Table S2b. The statistic of Pacbio subreads length distribution. Related to Figure 1.

Length (bp)	Num	Total length (bp)	Average length (bp)
0~2000	227,002	308,289,603	1,358
2000~4000	293,359	859,695,674	2,931
4000~6000	283,464	1,419,329,012	5,007
6000~8000	281,390	1,967,306,789	6,991
8000~10000	273,231	2,461,567,552	9,009
10000~12000	308,358	3,395,984,822	11,013
12000~14000	275,809	3,573,685,572	12,957
14000~16000	203,459	3,040,961,048	14,946
16000~18000	144,022	2,440,252,006	16,944
18000~	353,102	8,328,903,427	23,588
Total	2,643,196	27,795,975,505	10,516

Table S3. The assembly results of melon genome using different softwares. Related to Figure 1.

Software	Contig number	Contig length (bp)	Contig N50 (bp)	Contig N90 (bp)	Contig Max (bp)	GC%
Canu v1.5	755	365,394,387	1,016,639	267,218	9,266,155	33.82
DBG2OLC	1,328	389,219,408	821,979	180,906	4,725,009	33.80
Quickmerage	803	386,470,950	2,863,989	511,464	11,158,838	33.89

Table S4. Statistics of pseudochromosomes of melon. Related to Figure 1.

Group	Sequence Number	Sequence Length (bp)
Chr1	59	37,360,996
Chr2	24	25,498,186
Chr3	36	31,151,059
Chr4	60	34,816,742
Chr5	65	30,780,632
Chr6	55	37,833,529
Chr7	70	31,462,808
Chr8	68	35,445,645
Chr9	28	24,937,816
Chr10	54	28,136,047
Chr11	55	34,134,534
Chr12	63	29,233,345
Total Sequences Clustered (Ratio %)	637(72.22)	380,791,339(98.53)
Total Sequences Ordered and Oriented (Ratio %)	271(42.54)	363,764,534(95.53)

Table S5. Genome completeness evaluation based on short reads mapped to genome. Related to Figure 1.

Total reads	Mapped reads	Mapped(%)	Properly mapped reads	Properly mapped(%)
218,378,255	216,286,575	99.04	210,224,508	96.81

Table S6. Genome completeness evaluation based on all PacBio subreads mapped back to genome. Related to Figure 1.

Total Number	2,643,196
Total Length	2,026,171,729
Total Mapped Number	2,343,297(88.65)
Total Mapped_Length	24,691,702,398(88.83)
Mapping_identity	84.06
Properly_Mapped_number	1,898,351(71.82)
Properly_Mapped_length	18,225,688,665(65.57)
Properly_Mapped_identity	84.83

Table S7. Genome completeness evaluation based on CEGMA database. Related to Figure 1.

Species	Number of 458 CEGs* present in assembly	% of 458 CEGs present in assemblies	Number of 248 highly conserved CEGs present	% of 248 highly conserved CEGs present
Payzawat melon	448	97.82%	246	99.19%

Table S8. Genome completeness evaluation based on BUSCO database. Related to Figure 1.

Complete BUSCOs (C)	1,336
Complete and single-copy BUSCOs (S)	1,278
Complete and duplicated BUSCOs (D)	58
Fragmented BUSCOs (F)	30
Missing BUSCOs (M)	74
Total BUSCO groups searched	1,440

Table S9. The single base error evaluation of melon genome. Related to Figure 1.

Contig length (bp)	Correct base number (bp)	Error base number (bp)	Error base percentage (%)
386,470,950	386,469,646	1,304	0.0003374

Table S10. The position of centromeres in Payzawat. Related to Figure 1.

Chr	start	end	length
chr07	8,015,331	8,018,992	3,661
chr07	8,206,075	8,226,875	20,800
chr07	20,841,172	20,842,193	1,021
chr07	20,843,257	20,847,128	3,871
chr07	20,848,967	20,859,599	10,632
chr07	20,862,464	20,868,572	6,108
chr07	20,872,481	20,875,457	2,976
chr07	20,878,955	20,880,323	1,368
chr09	12,317,864	12,326,398	8,534
chr09	12,336,629	12,343,584	6,955
chr09	12,419,626	12,426,587	6,961
chr09	12,432,876	12,436,582	3,706
chr09	12,438,202	12,439,594	1,392
chr09	12,483,168	12,487,617	4,449
chr01	27,893,563	27,898,799	5,236
chr01	27,902,574	27,904,244	1,670
chr01	27,914,340	27,917,772	3,432
chr01	27,923,006	27,927,215	4,209
chr01	27,936,171	27,940,186	4,015
chr01	27,950,089	27,958,282	8,193
chr10	21,539,424	21,544,931	5,507
chr10	21,582,330	21,588,656	6,326
chr10	21,592,978	21,595,406	2,428
chr10	23,409,214	23,419,616	10,402
chr10	23,438,756	23,440,072	1,316
chr10	23,441,655	23,442,704	1,049
chr08	24,260,189	24,273,071	12,882
chr08	24,275,260	24,280,456	5,196
chr08	24,295,050	24,300,327	5,277
chr08	24,323,583	24,339,816	16,233
chr08	24,352,904	24,357,464	4,560
chr08	24,358,854	24,368,249	9,395
chr08	24,562,073	24,575,419	13,346
chr08	26,997,779	26,999,774	1,995
chr08	27,003,939	27,021,444	17,505
chr04	22,747,982	22,763,666	15,684
chr04	22,950,178	22,960,972	10,794
chr04	22,966,229	22,972,403	6,174

chr04	22,975,165	22,978,123	2,958
chr06	12,727,898	12,732,373	4,475
chr06	12,746,562	12,766,615	20,053
chr11	19,214,550	19,221,839	7,289
chr11	19,225,959	19,247,642	21,683
chr11	20,169,026	20,177,304	8,278
chr11	20,193,590	20,206,634	13,044
chr11	21,838,773	21,852,751	13,978
chr05	11,136,461	11,141,615	5,154
chr05	11,144,384	11,160,121	15,737
chr02	17,684,383	17,698,691	14,308
chr02	19,266,330	19,268,697	2,367
chr02	19,271,003	19,281,783	10,780
chr02	19,294,902	19,296,307	1,405
chr02	19,297,779	19,300,853	3,074
chr02	19,303,933	19,310,266	6,333
chr03	17,115,534	17,130,132	14,598
chr03	19,587,074	19,603,704	16,630
chr03	19,651,784	19,653,131	1,347
chr03	19,658,110	19,672,851	14,741
chr12	5,332,493	5,337,079	4,586
chr12	5,370,036	5,385,820	15,784
chr12	5,431,354	5,435,327	3,973
chr12	11,305,901	11,317,300	11,399
chr12	11,319,463	11,324,210	4,747
chr12	11,325,236	11,330,678	5,442
chr12	11,340,154	11,341,360	1,206
chr12	11,342,976	11,352,077	9,101
chr12	11,361,571	11,373,911	12,340
chr12	11,378,487	11,405,001	26,514
chr12	11,414,540	11,441,351	26,811
chr12	11,443,885	11,454,420	10,535
chr12	11,458,460	11,463,850	5,390
chr12	12,546,050	12,560,234	14,184
chr12	13,262,503	13,265,941	3,438
chr12	13,279,579	13,284,715	5,136
chr12	15,875,192	15,885,071	9,879
chr12	15,894,482	15,898,343	3,861
chr12	15,899,582	15,903,423	3,841
chr12	15,908,872	15,916,292	7,420

Table S11. The position of centromeres in CM3.6.1. Related to Figure 1.

Chr	start	end	length
chr03	17,742,757	17,743,802	1,045
chr08	27,672,447	27,675,819	3,372
chr08	27,712,504	27,714,162	1,658
chr08	27,717,811	27,719,191	1,380
chr08	29,909,421	29,910,698	1,277
chr08	29,933,035	29,936,649	3,614
chr02	20,259,278	20,260,332	1,054
chr02	21,870,709	21,871,714	1,005
chr02	21,874,072	21,875,685	1,613
chr11	19,614,632	19,615,904	1,272
chr11	19,620,451	19,622,053	1,602
chr11	19,623,517	19,626,128	2,611
chr11	20,612,742	20,620,499	7,757
chr11	20,640,710	20,642,256	1,546
chr11	20,649,687	20,651,263	1,576
chr11	20,667,175	20,670,878	3,703
chr11	20,674,239	20,682,558	8,319
chr06	16,344,750	16,346,423	1,673
chr07	3,841,902	3,844,347	2,445
chr07	3,846,355	3,847,591	1,236
chr07	6,351,604	6,355,252	3,648
chr12	10,596,545	10,598,804	2,259
chr12	10,604,391	10,609,560	5,169
chr12	10,615,471	10,617,219	1,748
chr12	10,630,371	10,632,002	1,631
chr12	10,633,459	10,637,214	3,755
chr12	10,638,910	10,641,712	2,802
chr12	10,654,436	10,655,923	1,487
chr12	10,659,565	10,662,153	2,588
chr12	10,663,300	10,665,685	2,385
chr12	10,675,727	10,684,566	8,839
chr12	10,703,341	10,707,125	3,784
chr12	10,709,139	10,712,579	3,440
chr12	10,718,792	10,720,687	1,895
chr12	10,727,683	10,730,544	2,861
chr12	10,734,364	10,736,114	1,750
chr12	10,743,571	10,745,328	1,757
chr12	10,746,758	10,748,320	1,562

chr12	10,759,308	10,761,076	1,768
chr12	10,763,116	10,765,444	2,328
chr09	12,397,946	12,399,622	1,676
chr09	12,401,997	12,403,402	1,405
chr09	12,425,831	12,427,816	1,985
chr09	12,433,047	12,435,085	2,038
chr09	12,530,564	12,531,613	1,049
chr04	22,568,462	22,571,832	3,370
chr04	22,809,439	22,811,373	1,934
chr04	22,818,031	22,819,084	1,053
chr10	26,646,135	26,648,001	1,866
chr10	26,649,714	26,653,004	3,290

Table S12. The position of telomeres in Payzawat. Related to Figure 1.

Chr	start	end
chr01	18945	19019
chr01	18945	19098
chr01	20909	20962
chr01	20913	20962
chr03	247641	252634
chr04	1435	4527
chr05	3854888	3861842
chr07	2790259	2790909
chr08	490689	490759
chr09	225715	225784
chr10	13359	13602
chr12	947196	947242
chr03	30117021	30117116
chr04	33368710	33374109
chr07	29453786	29453843
chr09	24250739	24262802
chr12	27486643	27520640

Table S13. The position of telomeres in CM3.6.1. Related to Figure 1.

Chr	start	end
chr01	1,364	1,417
chr04	131,820	131,878
chr05	108	225
chr06	36,915,748	36,915,775
chr10	544,858	544,886

Table S14. The repeat elements of melon genome. Related to Figure 1.

Type	Number	Length（bp）	Percentage (%)
ClassI/?/?	551	271,757	0.07
ClassI/DIRS/?	21,562	17,936,642	4.64
ClassI/DIRS/DIRS	3	149	0.00
ClassI/LARD/?	53,700	19,381,169	5.01
ClassI/LINE/?	2,162	955,712	0.25
ClassI/LINE/I	11	738	0.00
ClassI/LINE/Jockey	9	522	0.00
ClassI/LINE/L1	8,158	3,066,023	0.79
ClassI/LINE/R2	10	462	0.00
ClassI/LINE/RTE	9	689	0.00
ClassI/LTR/?	2,012	908,864	0.24
ClassI/LTR/Copia	76,236	48,966,451	12.67
ClassI/LTR/Gypsy	109,600	66,674,086	17.25
ClassI/LTR/Retrovirus	1	101	0.00
ClassI/PLE/Penelope	408	40,059	0.01
ClassI/PLE|LARD/?	1,025	238,717	0.06
ClassI/SINE/?	5,601	1,074,120	0.28
ClassI/TRIM/?	768	319,729	0.08
ClassII/?/?	1,164	193,622	0.05
ClassII/?/Academ	2	83	0.00
ClassII/?/Ginger2/TDD	2	695	0.00
ClassII/?/ISL2EU	1	48	0.00
ClassII/?/Kolobok	628	60,431	0.02
ClassII/?/MuDR	5,757	3,660,728	0.95
ClassII/?/Novosib	34	4391	0.00
ClassII/?/Sola	7	600	0.00
ClassII/Crypton/Crypton	830	352,479	0.09
ClassII/Helitron/Helitron	7,524	1,209,828	0.31
ClassII/MITE/?	2,227	429,934	0.11
ClassII/Maverick/?	2,878	1,140,186	0.30
ClassII/TIR/?	14,406	8,560,416	2.22
ClassII/TIR/CACTA	23,208	15,115,707	3.91
ClassII/TIR/P	303	23,952	0.01
ClassII/TIR/PIF-Harbinger	7,795	3,646,425	0.94
ClassII/TIR/PiggyBac	10	610	0.00

ClassII/TIR/Tc1-Mariner	25	2,060	0.00
ClassII/TIR/hAT	13,809	4,331,570	1.12
PotentialHostGene	13,128	2,633,731	0.68
SSR	5,317	1,040,848	0.27
Unknown	135,682	38,668,955	10.01
Total without overlap	516,563	192,457,182	49.80

Table S15. Summary of the melon genome gene model prediction. Related to Figure 1.

Method	Software and Species		Gene number
Ab initio		Genscan	21,436
		Augustus	23,111
		GlimmerHMM	23,925
		GeneID	34,013
		SNAP	42,865
	GeMoMa	*Cucumis sativus (Cultivar: Borszczagowski)*	16,909
		Cucumis sativus (Cultivar: 9930)	20,171
Homology-based		*Cucumis melo*	21,712
EST/Unigene		PASA	39,751
Integration		EVM	22,924

Table S16. Statistics of the melon genome gene model prediction. Related to Figure 1.

Software	Gene Number	Total length (bp)	Average gene length (bp)	Total exon length (bp)	Average exon length (bp)	Total Intron Length (bp)	Average Intron length (bp)
EVM	22,924	102,944,993	4,491	29,654,362	238	59,893,433	480

Table S17. The gene-set evaluation by mapping mRNA reads to genome. Related to Figure 1.

Type	BaseNum (bp)	Percentage (%)
Exon	6,547,111,128	88.97%
Intron	366,647,491	4.98%
Intergenic	445,330,510	6.05%
Total	7,359,089,129	100

Table S18. Summary of the ncRNAs in melon geneme. Related to Figure 1.

RNA classification	Number	Family
miRNA	75	19
rRNA	443	4
tRNA	717	24

Table S19. Summary of the pseudogenes in melon genome. Related to Figure 1.

RNA classification	Number	Total length	Average Length
Frameshift	740	2,256,944	3,050
Stop codon termination	1,694	5,177,533	3,056
Total	2,434	7,434,477	3,054

Table S20. The gene functional annotation of melon. Related to Figure 1.

Database	Annotated number	Percentage (%)
KOG	8,596	37.5
GO	12,436	54.25
KEGG	7,582	33.07
TrEMBL	22,413	97.77
nr	22,492	98.12
All Annotated	22,506	98.18

Table S21. The valid data evalution of Hi-C clean reads. Related to Figure 1.

Type		Reads Number	Ratio(%)
Total Read Pairs		164,495,209	100
Mapped Reads Pairs		149,968,147	91.17
Unique Mapped Read Pairs		76202174	46.32
Unique Mapped Read Pairs	Valid Interaction Pairs	53,271,510	69.91
	Dangling End Pairs	9,199,190	12.07
	Re-ligation Pairs	1,172,025	1.54
	Self-cycle Pairs	8,710,138	11.43
	Dumped Pairs	3,849,311	5.05

Table S22. Summary of the genome correction by Hi-C data. Related to Figure 1.

Statistics	Merged Assembly congtis	Corrected contigs
Contig number	803	863
Contig length	386,470,950	386,470,950
Contig N50 (bp)	2,863,989	2,316,192
Contig N90 (bp)	511,464	393,785
Contig Max (bp)	11,158,838	6,858,417
Gap number	0	0

Table S23. Statistics of aligned sequences, SNPs and Indels in Payzawat from Payzawat and CM3.6.1 whole-genome sequence comparison. Related to Figure 2 and 3.

	Syntenic block length	No. of genes
One-to-One syntenic blocks	296,593,814 bp(76.7%)	19,110
SNPs	1,761,822	9,795
Insertion	371,560	7,779
Deletion	363,926	8,216

Table S24. Genome distribution of SNPs and Indels within one-to-one syntenic blocks in Payzawat from Payzawat and CM3.6.1whole-genome sequence comparison. Related to Figure 2 and 3.

	SNP			SNP within one-to-one syntenic blocks		
region	Number	Percent	No. of affected genes	Number	Percent	No. of affected genes
5'UTR	109,259	6.201477788	6,055	69,714	7.732442451	4,386
CDS	33,636	1.909159949	6,971	20,591	2.283884478	4,771
Intron	168,487	9.563224889	7,460	109,455	12.14038053	5,467
3'UTR	109,982	6.242514851	6,438	73,847	8.190860913	4,701
Intergenic	1,340,458	76.08362252		627,971	69.65243163	-
Total	1,761,822	100	9,795	901,578	100	7,046

	Deletion			Deletion within one-to-one syntenic blocks		
region	Number	Percent	No. of affected genes	Number	Percent	No. of affected genes
5'UTR	23,943	6.579084759	4655	14,562	8.125073233	3,444
CDS	2,517	0.691624121	1239	1,335	0.744882074	736
Intron	37,340	10.26032765	6099	22,830	12.73832042	4,538
3'UTR	23,125	6.354313789	4715	14,789	8.251731084	3,469
Intergenic	277,001	76.11464968	-	125,707	70.13999319	-
Total	363,926	100	8216	179,223	100	6,081

	Insertion			Insertion within one-to-one syntenic blocks		
region	Number	Percent	No. of affected genes	Number	Percent	No. of affected genes
5'UTR	23,050	6.20357412	4,397	13,177	7.409427522	3,227
CDS	2,031	0.546614275	966	924	0.51956523	546
Intron	37,318	10.04359996	5,761	21,543	12.11362959	4,274
3'UTR	23,436	6.307460437	4,574	14,329	8.057197159	3,391
Intergenic	285,725	76.89875121	-	127,868	71.9001805	-
Total	371,560	100	7,779	177,841	100	5,749

Table S25. Position distribution of structural variation. Related to Figure 2 and 3.

	Type No.	5'UTR	CDS	Intron	3'UTR	Intergenic	Total
Structural variation	GAP	2,507	995	3,595	2,386	21,471	26,067
	DUP	8	9	12	8	68	83
	BRK	114	115	99	107	338	459
	JMP	340	325	403	317	3,455	4,021
	INV	325	331	386	299	2,935	3,481
	SEQ	1,351	1,086	1,636	1,277	13,004	15,279
Structural variation within one-to-one syntenic blocks	GAP	491	73	670	438	4,381	5,226
	DUP	0	0	0	0	0	0
	BRK	0	0	0	0	0	0
	JMP	8	8	9	6	61	73
	INV	3	0	2	1	19	23
	SEQ	132	75	155	115	1,372	1,633

Table S26. Statistics of genes with large variation. Related to Figure 2 and 3.

Type No. of affected genes	No.	Percent
GAP	906	76.3912
DUP	0	0
BRK	0	0
JMP	19	1.60202
INV	4	0.337268
SEQ	270	22.7656
Total	1186	

Table S27. Large inversions detected in chromosome chr06. Related to Figure 2.

Payzawat chr	Payzawat start	Payzawat end	Payzawat length	CM3.6.1 chr	CM3.6.1 start	CM3.6.1 end	CM3.6.1 length
chr06	16,635,346	18,619,220	1,983,875	chr06	17,483,805	19,510,221	2,026,417
chr06	18,682,858	24,319,858	5,637,001	chr06	19,585,830	25,280,518	5,694,689
chr06	24,404,623	28,895,149	4,490,527	chr06	25,796,221	30,486,008	4,689,788
chr06	28,975,754	30,534,865	1,559,112	chr06	30,835,567	32,330,124	1,494,558
chr06	30,563,968	36,185,168	5,621,201	chr06	29,270,981	38,297,372	9,026,392

Table S28. Validation of large inversions detected in chromosome chr06. Related to Figure 2.

Payzawat chr	Payzawat start	Payzawat end	Left breakpoint start	Left breakpoint end	Right breakpoint start	Right breakpoint end
chr06	16,635,346	18,619,220	16,557,453	16,635,346	18,619,220	18,682,858
chr06	18,682,858	24,319,858	18,619,220	18,682,858	24,319,858	24,344,072
chr06	24,404,623	28,895,149	24,355,748	24,404,623	28,895,149	28,975,754
chr06	28,975,754	30,534,865	28,895,149	28,975,754	30,534,865	30,545,753
chr06	30,563,968	36,185,168	30,534,865	30,545,753		

Table S29. Details of samples used for RNAseq analysis. Related to Figure 1 and 2.

SRR	Library strategy	Description	rind thickness
SRR6320593	RNAseq	PI161375 (non-climacteric) fruit flesh and peel at 10 days post anthesis	thin rind
SRR7343307	RNAseq	PI161375 (non-climacteric) fruit flesh and peel at 20 days post anthesis	thin rind
SRR5405113	RNAseq	PI161375 (non-climacteric) fruit flesh and peel at 40 days post anthesis	thin rind
SRR5405110	RNAseq	Vedrantais (climacteric) fruit flesh and peel at 10 days post anthesis	thick rind
SRR5405109	RNAseq	Vedrantais (climacteric) fruit flesh and peel at 20 days post anthesis	thick rind
SRR5405108	RNAseq	Vedrantais (climacteric) fruit flesh and peel at 30 days post anthesis	thick rind
SRR5405107	RNAseq	Vedrantais (climacteric) fruit flesh and peel at 40 days post anthesis	thick rind
SRR1501088	RNAseq	C. melo var ameri, cv ‘Flavor No. 4’ fruits at 0 days post anthesis	thick rind
SRR1501219	RNAseq	C. melo var ameri, cv ‘Flavor No. 4’ fruits at 10 days post anthesis	thick rind
SRR1503342	RNAseq	C. melo var ameri, cv ‘Flavor No. 4’ fruits at 20 days post anthesis	thick rind
SRR1503343	RNAseq	C. melo var ameri, cv ‘Flavor No. 4’ fruits at 30 days post anthesis	thick rind
SRR1503344	RNAseq	C. melo var ameri, cv ‘Flavor No. 4’ fruits at 40 days post anthesis	thick rind

Table S30. Summary of resequencing samples. Related to Figure 4 and 5.

Sample NO	Accession name	Group	Orgin	Botanical variety
R13	African Horn Melon	wild relative species	African	Cucumis metulifeus
R22	PI 614512	wild	India	C.*agrestis* var.*agrestis*
R12	Agretis	wild	India	C.*agrestis* var.*agrestis*
R26	PI 180283	wild	India	C.*agrestis* var.*agrestis*
R32	PI 614307	wild	India	C.*agrestis* var.*agrestis*
R31	PI 614173	wild	India	C.*agrestis* var.*agrestis*
R33	PI 614309	wild	India	C.*agrestis* var.*agrestis*
R30	PI 536473	wild	Maldives	C.*agrestis* var.*agrestis*
R28	PI 406737	wild	Costarica	C.*agrestis* var.*agrestis*
R29	PI 532829	wild	Shanxi, China	C.*agrestis* var.*agrestis*
R34	Mapaogua	wild	Shandong China	C.*agrestis* var.*agrestis*
R11	Kangua	wild	China	*C.agrestis* var.*chinensis*
R24	Zhonghuacaigua	cultivar/landrace	Henan, China	*C.agrestis* var.*conomon*
R01	Xianggua	wild	China	*C.agrestis* var.*chinensis*
R09	PI 161375	landrace	Korea	*C.agrestis* var.*chinensis*
R17	Yangjiaosu	cultivar/landrace	Hebei, China	*C.agrestis* var.*chinensis*
R15	Huangpimiangua	cultivar/landrace	Henan, China	*C.agrestis* var.*chinensis*
R20	Huangjingua	cultivar/landrace	Japan	C.*agrestis* var.*chinensis*
R14	Tinglinxuegua	cultivar/landrace	Shanghai, China	*C.agrestis* var.*chinensis*
R38	Baizhuogua	cultivar/landrace	Zhejiang, China	*C.agrestis* var.*chinensis*
R18	Zhimasu	cultivar/landrace	Shanxi, China	*C.agrestis* var.*chinensis*
R39	Bingtangzi	cultivar/landrace	Shandong, China	*C.agrestis* var.*chinensis*
R08	Yagua	cultivar/landrace	Northeast China	*C.agrestis* var.*chinensis*
R16	Balixiang	cultivar/landrace	Jilin, China	*C.agrestis* var.*chinensis*
R19	Tiebaqing	cultivar/landrace	Liaoning, China	*C.agrestis* var.*chinensis*
R07	PI 414723	wild	India	C.*agrestis* var.*momordica*
R04	PI 371795	wild	India	C.*agrestis*.var *momordica*
R06	PI 313970	wild	India	C.*agrestis*.var *momordica*
R03	PI 446928	cultivar	Isreal	C.*agrestis*.var *momordica*

R36	MR-1	breeding material	USA	C.*agrestis var.momordica*
R37	PI 124111	wild	India	*C.agrestis* var.*momordica*
R02	Im-2	landerce	Italy	*C.melo* var.*chandalak*
R23	Edisto 47	cultivar	America	*C.melo* var.*reticulatus*
R35	PI 446929	cultivar	Isreal	*C.melo* var.*chandalak*
R25	Fcouss	landerce	France	*C.melo* var.*flexuosus*
R41	Tashikehong	Landrace	Xinjiang, China	*C.melo* var.*chandalak*
R40	Im41	cultivar/landrace	Italy	*C.melo* var.*inodorus*
R05	PI 234607	cultivar/landrace	South Africa	*C.melo* var.*inodorus*
R10	Pil de sapo	cultivar/landrace	Spain	*C.melo* var.*inodorus*
R49	Boxiekexin	Landrace	Xinjiang, China	C.*melo* var.*cassaba*
R21	PI 222187	landerce	Afghanistan	*C.melo* var.*flexuosus*
R27	Minoo	cultivar/landrace	Iran	*C.melo* var.*ameri*
R43	Bokezade	Landrace	Xinjiang, China	*C.melo* var.*ameri*
R46	Mizigua	Landrace	Xinjiang, China	*C.melo* var.*ameri*
R44	Baibicui	Landrace	Xinjiang, China	*C.melo* var.*ameri*
R48	Pishan	Landrace	Xinjiang, China	*C.melo* var.*ameri*
R42	Naxigan	Landrace	Xinjiang, China	*C.melo* var.*ameri*
R45	Huapijinbangzi	Landrace	Xinjiang, China	*C.melo* var.*ameri*
R47	Hongxincui	Landrace	Xinjiang, China	*C.melo* var.*ameri*
R50	Huanghuapibairoumijigan	Landrace	Xinjiang, China	*C.melo* var.*ameri*

Table S31. Statistics of reads and mapping for 50 accessions. Related to Figure 4 and 5.

Accession	Total_reads	Mapped(%)	Properly_mapped(%)	Average depth	Coverage 1X(%)	Coverage 5X(%)	Coverage 10X(%)
R01	90,443,068	98.25	93.31	18	87.09	80.45	69.9
R02	109,867,078	98.69	95.47	22	88.33	84.04	77.05
R03	96,454,242	98.51	94.64	19	87.78	82.15	73.13
R04	92,316,822	98.41	94.21	19	87.59	82.45	73.52
R05	88,244,156	98.98	92.66	16	89.13	81.7	68.35
R06	101,321,854	98.51	94.54	20	87.56	81.68	72.83
R07	88,429,654	98.51	94.7	17	87.24	79.23	67.68
R08	106,328,706	97.94	93.62	22	86.85	82.06	75.08
R09	90,979,806	98.14	93.94	19	86.53	80.94	71.58
R10	101,505,104	98.96	93.53	18	89.26	81.99	69.88
R11	95,639,144	98.31	94.28	18	86.24	76.97	65.43
R12	95,063,612	98.26	94.21	17	86.65	78.66	67.07
R13	97,975,978	42.1	33.76	12	34.72	24.6	19.56
R14	107,135,906	98.29	94.39	20	86.59	79.36	69.85
R15	101,394,312	98.11	94.25	20	86.77	80.96	72.33
R16	93,361,670	98.31	92.16	17	86.43	76.19	64.13
R17	92,116,208	98.23	92.09	18	86.67	78.38	67.36
R18	87,152,822	98.35	94.06	17	85.66	75.79	63.62
R19	101,719,444	98.15	93.85	20	86.55	78.89	69.21
R20	102,527,186	98.42	93.74	19	86.5	77.16	66.04
R21	91,825,482	98.99	95.31	18	88.89	82.32	71.42
R22	105,856,152	98.08	93.56	22	88.02	83.49	76.46
R23	100,373,426	98.84	94.22	19	88.97	82.28	72.58
R24	92,555,320	98.34	94.12	18	86.58	78.78	68.09
R25	91,196,176	98.87	95.5	17	88.16	79.16	66.85
R26	106,718,396	98.26	93.58	20	86.99	80.67	71.63
R27	90,552,366	99.09	96.12	17	88.2	77.49	65.1

R28	88,901,202	98.26	94.11	16	85.84	75.46	61.97
R29	101,792,584	98.64	94.52	19	87.46	79.95	69.53
R30	95,951,796	98.37	94.13	17	86.78	79.1	67.64
R31	101,500,506	98.49	94.59	18	87.07	80.41	69.74
R32	106,034,336	98.34	94.49	20	87.22	80.63	71.64
R33	95,550,544	98.41	94.4	17	87.15	79.74	68.17
R34	94,549,986	98.42	94.25	18	86.28	77.84	66.69
R35	91,119,776	98.89	95.63	18	88.26	80.47	69.37
R36	96,869,602	98.73	95.51	18	87.02	78	66.97
R37	107,651,060	98.82	95.69	19	88.18	80.54	70.54
R38	98,489,908	98.41	94.27	18	86.74	79.57	69.12
R39	99,096,020	98.22	93.99	19	86.8	79.42	69.37
R40	103,471,468	98.98	95.01	19	89.04	82.79	72.86
R41	98,252,796	97.75	94.59	19	88.16	79.92	69.32
R42	89,199,864	94.09	90.84	17	88.88	80.41	68.02
R43	85,011,750	98.62	95.68	16	88.55	78.25	64.93
R44	95,758,812	88.17	85.63	18	89.27	83.75	73.4
R45	87,896,514	95.77	92.38	17	88.37	78.02	65.77
R46	94,565,194	98.36	95.6	18	88.88	81.14	70.3
R47	93,635,898	96.19	92.45	18	88.7	80.16	68.62
R48	97,517,576	89.58	86.74	18	88.89	80.35	68.93
R49	105,886,098	97.32	93.87	20	89.49	83.76	74.19
R50	100,271,900	95.99	93.36	19	89.56	83.14	72.8

Table S32. Statistics of SNPs for 50 accessions. Related to Figure 4 and 5.

Accession	SNP number	Transition	Transversion
R01	1299330	894092	405238
R02	746957	512928	234029
R03	967729	665461	302268
R04	1115180	764894	350286
R05	597754	409376	188378
R06	1100618	756192	344426
R07	1091484	750497	340987
R08	1323638	910416	413222
R09	1296099	891730	404369
R10	599633	410889	188744
R11	1286260	887636	398624
R12	1340595	923456	417139
R13	1397537	857300	540237
R14	1306832	901132	405700
R15	1321611	909679	411932
R16	1292906	893231	399675
R17	1294154	892706	401448
R18	1272472	879242	393230
R19	1299286	896103	403183
R20	1285367	886944	398423
R21	565455	387673	177782
R22	1604550	1102928	501622
R23	773922	531617	242305
R24	1313675	905988	407687
R25	818625	564057	254568
R26	1364308	938448	425860
R27	447215	307781	139434
R28	1303077	899170	403907
R29	1055085	726906	328179
R30	1391303	959524	431779
R31	1330168	916129	414039
R32	1247410	859287	388123
R33	1271175	876475	394700
R34	1295543	893604	401939
R35	677096	465094	212002
R36	878104	606031	272073
R37	828899	571299	257600
R38	1312911	904489	408422

R39	1303084	897891	405193
R40	527224	360712	166512
R41	544124	373776	170348
R42	339382	231687	107695
R43	337273	231665	105608
R44	335147	229099	106048
R45	299581	205159	94422
R46	322078	220150	101928
R47	289933	198764	91169
R48	275650	188896	86754
R49	372668	254272	118396
R50	274280	186742	87538

Table S33. Statistics of structure variation for 50 accessions. Related to Figure 4.

Accession	SV	INS	DEL	INV	ITX	CTX	UN
R01	27886	9714	12359	637	637	4513	26
R02	22949	9549	7466	780	555	4572	27
R03	20644	5679	9071	573	627	4667	27
R04	22915	6992	10158	633	588	4514	30
R05	23763	13839	5065	462	643	3731	23
R06	22768	6359	10447	563	584	4792	23
R07	19769	5323	8832	499	597	4491	27
R08	29659	10378	12856	745	721	4937	22
R09	30381	11494	13095	665	581	4518	28
R10	23462	13054	5238	457	627	4059	27
R11	27914	10466	11868	473	626	4455	26
R12	23753	6012	11803	508	676	4715	39
R13	8225	1592	2745	149	198	3502	39
R14	29825	12141	11718	506	645	4789	26
R15	28206	9820	12270	537	684	4870	25
R16	25673	10878	10967	503	616	2685	24
R17	24345	8829	11770	522	593	2602	29
R18	25970	9205	11438	468	564	4273	22
R19	29133	11246	12270	520	627	4444	26
R20	28005	11932	10495	487	618	4451	22
R21	16805	6058	5911	384	550	3874	28
R22	28506	7817	14313	728	746	4859	43
R23	25237	12445	7425	437	624	4284	22
R24	26891	10339	10915	505	611	4494	27
R25	20514	7685	7695	371	539	4196	28
R26	29538	11451	11963	543	670	4880	31
R27	17668	8241	4409	332	461	4209	16
R28	22509	6949	10324	493	652	4063	28
R29	25747	10522	9753	461	576	4410	25
R30	25294	7378	12256	525	698	4409	28
R31	27038	8880	12300	509	689	4641	19
R32	26927	9340	11402	560	686	4907	32
R33	24917	7568	11678	511	663	4475	22
R34	27417	10921	11002	514	630	4323	27
R35	16822	4580	6890	392	583	4355	22
R36	17871	4246	7995	428	582	4592	28
R37	17838	4491	7680	434	550	4659	24
R38	27272	9670	11834	515	626	4599	28

R39	29733	11863	11902	512	647	4775	34
R40	24479	13335	5691	388	562	4476	27
R41	19942	8975	5502	356	552	4539	18
R42	18477	9621	3904	319	477	4144	12
R43	15931	7310	3784	302	434	4078	23
R44	12833	3560	4185	362	477	4226	23
R45	18488	9953	3672	305	479	4064	15
R46	13626	4427	3973	330	457	4424	15
R47	21010	12482	3621	299	490	4100	18
R48	19897	11420	3356	263	465	4375	18
R49	22614	12704	4443	324	528	4584	31
R50	12859	3696	3545	340	503	4756	19

Table S34. 275 mutations implciated in the contrasting phenotypes between wild and cultivated populations. Related to Figure 5.

Transparent Methods

1 Genome sequencing and assembly

1.1 Sample preparation and sequencing

The strain for sequencing was a cultivated one (*Cucumis melo* L. var. inodorus) from Payzawat county in Kashgar, Sinkiang. Usually the Payzawat natives call it Payzawat melon and the others call it Kalakesai. The DNA of the melon was extracted from leaf following a previous published protocol.

1.2 Genome size estimation and assembly

A total of 32.53 Gb of Illumina PE (2×150 bp) clean bases were generated with about 81-fold coverage (see Tables S1). The genome survey analysis was performed using “kmer freq stat” software (developed by Biomarker Technologies). The highest peak in the k-mer distribution curve was at 64. The peak at depth of more than 128 was a repetitive peak. Finally, the melon genome size was estimated to be 398.57 Mb, with about 0.03% heterozygosity and 43.39% repeat sequences (see Figure S1).
For SMRT sequencing, a total of 4,057,884 polymerase reads (30.78 Gb) were generated on the PacBio RSII platform (see Tables S2a and S2b). In quality control step, only subreads with length more than 500 bp and RQ value higher than 0.75 were retained for future analysis. Finally, A total of 2,643,196 PacBio post-filtered reads which accounting for approximately 27.80 Gb sequencing data were generated. The subreads N50 reached 13,947 and the average subread length was 10.52 kb. Canu (v1.5)(Koren S, et al., 2017) assembler and DBG2LOC(Ye C, Hill CM, Wu S, Ruan J, Ma ZS, 2016) were used for *de novo* assembly. To improve the assembly result, Quickmerge(Chakraborty M, Baldwin-Brown JG, Long AD, Emerson JJ, 2016) software was used to merge the two genome assemblies (see Tables S3). The genome was first polished by Quiver (--minLength 3000 --maxHits 1) and followed by three round Pilon (v1.22, --mindepth 20 --fix base)(Walker BJ, et al., 2014) using the Illumina short reads.

1.3 Chromosome construction and evaluation

To anchor the contigs into pseudochromosomes, we performed HI-C experiments. A total of 49.07 Gb clean data were sequenced using the Illumina X-Ten platform, with about 127-fold coverage (see Table S21). The clean reads were mapped to the contigs using BWA aln method with default parameters and 46.32% reads were uniquely mapped. 69.91% of the unique mapped reads were identified as the valid

interaction read pairs with paired *Hin*dIII restriction site by HiC-Pro(Servant N, et al., 2015) (see Table S21). Before anchoring the contigs, we first performed a contigs correction step. In this step, the contigs were firstly interrupted at 500 kb window, and then the valid linked reads were mapped to the interrupted contigs. Once the broken contigs could not be linked back to the original contigs, the original contigs were interrupted at a low coverage site. After correction, the contig N50 went to 2.31 Mb (see Table S22). Next, the pseudochromosomes were constructed using LACHESIS(Burton JN, et al., 2013) software with: CLUSTER MIN RE SITES = 71, CLUSTER MAX LINK DENSITY = 2, CLUSTER NONINFORMATIVE RATIO = 2, ORDER MIN N RES IN TRUNK = 59, and ORDER MIN N RES IN SHREDS = 59.

1.4 Genome assembly

The assembly completeness was assessed by means of three data sets: Genetic map, PE short reads, Pacbio subreads, CEGMA, and BUSCO. To evaluate the quality of our new assembly, the short reads used for estimation of genome size were realigned to the assembled genome using the bwa mem method with default parameters(see Table S5)(Li H, Durbin R, 2010). PacBio subreads were aligned to the assembly using blasr with parameters “-bestn 1 -minPctIdentity 70 -nproc 4”(see Table S6). Besides, we found that the single-base error rate was 0.0003374% (see Table S9), suggesting that the base of the genome was accurate. Genome completeness was also assessed using the core eukaryotic gene-mapping approach (CEGMA v2.5)(Parra G, 2007). It provides a rapid method of assessing genome completeness because it comprises a set of highly conserved, single-copy genes, present in all eukaryotes. CEGMA contains 458 core eukaryotic genes (CEGs) and among them 248 are highly-conserved CEGs. The BUSCO (Version 2) program was run against the embryophyta_odb9 dataset with the default parameters.

1.5 Centromere and telomere identification

Melon-specific CentM repeats (GenBank accession no. 3929695) were identified through blasting (BLAST, Version 2.2.31, E-value < 1×10^{-5}) search CentM sequences against the genome sequences (centromere repositioning in cucurbit species: Implication of the genomic impact from centromere activation and inactivation, Organization of highly repetitive satellite DNA of two Cucurbitaceae species (*Cucumis melo* and *Cucumis sativus*)). Repeats shorter than 1,000 bp were discarded. The repeat clusters between 1000 bp or overlapped clustered were merged. Telomeric repeats (TTTAGGG/CCCTAAA) were identified by tandem repeat finder (TRF) (Version 4.07b)(G. Benson, 1999).

2 Genome annotation

2.1 Repeat content identification

Both homolog and *de novo* strategies were applied to identify the repetitive sequence in melon genome. There were four *de novo* prediction software suites, including RepeatScout(Price AL, Jones NC, Pevzner PA, 2005), LTR-FINDER(Xu Z, Wang H, 2007), MITE-Hunter(Han Y, Wessler SR, 2010), and PILER-DF(Edgar RC, Myers EW, 2005), that were adopted for *ab initio* prediction. RepeatScout can find all repeat classes. LTR-FINDER was used to predict locations and structure of full-length LTR retrotransposons. MITE-Hunter was used to discover miniature inverted-repeat transposable elements (MITEs) from genomic sequences. PILER-DF is suitable when finding repeated elements such as satellites and transposons. Results from all *ab initio* predictions were combined to form a repetitive sequence library. The library was then merged with RepBase(Bao W, Kojima KK, Kohany O, 2015) and classified into different categories by the PASTEClassifier.py script included in REPET. The repetitive sequences in melon genome were identified by homolog searching in that database through RepeatMasker (Tarailo-Graovac M, Chen N, 2009).

2.2 Gene model, ncRNA and pseudogene prediction

Gene model annotation was performed using a combination of three methods: *ab initio* prediction, homology-based gene prediction, and transcript evidence from RNA-seq data. The *ab initio* prediction was conducted using five different suites of software: Genscan(Burge C, Karlin S, 1997), Augustus v2.4(Stanke M, Waack S, 2003), GlimmerHMM v3.0.4(Majoros WH, Pertea M, Salzberg SL, 2004), GeneID v1.4(Blanco E, Parra G, Guigo R, 2007), SNAP(version 2006-07-28)(Korf I, 2004), and GeMoMa (v1.3.1)(Keilwagen J, et al., 2016) was employed for gene prediction based on homologous genes, using model training based on coding sequences from *Arabidopsis thaliana*, *Oryza sativa*, *Cucumis sativus* (Cultivar: Borszczagowski), *Cucumis sativus* (Cultivar: 9930), and the previously sequenced *Cucumis* melon. The RNA-seq reads generated from various tissues of melon were assembled without a reference genome using Hisat v2.0.4(Kim D, Langmead B, Salzberg SL, 2015) and Stringtie v1.2.3(Pertea M, et al., 2015), then the unigenes were used to predict genes using PASA v2.0.2(Campbell MA, et al., 2006). Finally, we used EVM v1.1.1(Haas BJ, et al., 2008) to combine the results of the three methods. The ncRNAs were also predicted including miRNAs, tRNAs and rRNAs. tRNAs was detected by using tRNA-scan-SEM (version 1.23)(Lowe TM, Eddy SR, 1997). The miRNAs and rRNAs were found based on sequence alignment using BLASTN v2.26 with an e-value of less than 1×10^{-10} and Infernal v1.1(Nawrocki EP, Eddy SR, 2013) against Rfam v12.0(Nawrocki EP, 2015) database. A total of 1,235 non-coding RNAs were also identified in our melon assembly, including 75 microRNAs of 19 families, 443 rRNAs

of four families, and 717 tRNAs of 24 families (Table S18). The GeneWise(Birney E, Clamp M, Durbin R, 2004) software was used to identify pseudogenes, and a total of 2,434 pseudogenes were identified in melon genome (Tables S19).

2.3 Gene functional annotation analysis

Gene function was annotated by comparing their protein sequences against a number of protein sequence databases, including: Nr (NCBI non-redundant protein sequences), Nt (NCBI non-redundant nucleotide sequences), Pfam (Protein family); KOG (Clusters of Orthologous Groups of proteins), Swiss-Prot (a manually annotated and reviewed protein sequence database), KO (KEGG Ortholog database), and GO (Gene Ontology).

3 Whole-genome sequencing comparison

A whole-genome comparison between Payzawat and CM3.6.1 was performed using nucmer module of MUMmer package (version 4.0)(Marcais, G. et al., 2018). Structural variations were identified from the one-to-one syntenic blocks.

4 Resequencing and diversity analysis

4.1 Library construction and sequencing

A total of 49 accessions were collected (Table S30). Fresh young leaves were collected from each individual and immediately frozen in liquid nitrogen. DNA was extracted using the CTAB method(Murray MG, Thompson WF, 1980). Some 5 ug DNA for each individual could be used for library construction with *c*. 350 bp insert size. Libraries were sequenced on an Illunima Hiseq X Ten (2 x 150 bp). Raw reads were subjected to removal of adaptors and trimmed of low-quality bases and then 599.39-Gb clean data were obtained (approximately 12X coverage for each individual).

4.2 Reads mapping and variants calling

High-quality PE reads for each accession were mapped to the genome using the BWA program (Version 0.7.10, mapping method: MEM) with default parameters. Duplicated reads were discarded using the MarkDuplicates utility in Picard(http://sourceforge.net/projects/picard/). Variants were called using the HaplotypeCaller module in GATK (version 3.1.1)(McKenna A, et al., 2010). To obtain high-quality variants, stringent filtering was performed as follows: 1) clusterSize 2 clusterWindowSize 5; 2) QUAL < 30; 3) QD < 2.0; 4) MQ < 40; 5) FS > 60.6. 2,702,589 high-quality SNPs and 370,207 indels were retained for further analysis.

The identified SNPs and indels were annotated using SnpEff software (Version 3.6c)(Cingolani P, et al., 2012). BreakDancer-1.1(Chen K, et al., 2009) was used to identify large structural variants(see Table 33).

4.3 Population diversity

Population diversity was analysed using three methods, including phylogenetic tree construction, population stratification using ADMIXTURE(Alexander D H, Novembre J, Lange K, 2009), and high-quality SNPs (MAF = 0.05, missing rate = 0.5) were used to construct the phylogenetic relationships among 49 accessions using MEGA X(Kumar, Sudhir, et al., 2018) with a neighbour-joining method with Kimura 2-parameter model and 1,000 bootstrap replicates.
Population stratification among 49 accessions was inferred using ADMIXTURE software(Alexander D H, Novembre J, Lange K, 2009). Cross-validation error was tested for K (the most likely number of clusters) from 2 to 5 and the population with the smallest cross-validation error was chosen and results was plotted for K = 2 to K = 5.

4.4 Linkage disequilibrium (LD)

A total of 2,248,795 high-quality SNPs (MAF = 0.05, missing rate = 0.2) in 49 accessions were used to perform LD using Software plink(Purcell S, et al., 2007) through calculating the squared correlation coefficient (r^2) between any two SNPs within a 100 kb window.

4.5 Selective sweep

SNPs with minor allele frequency below 5% and missing rate above 0.2 were excluded. Software PopGenome(Pfeifer B, et al., 2014) was used to calculate Fst and pai with a 100 kb sliding window and s step size of 10 kb.

Supplemental references

Chakraborty M, Baldwin-Brown JG, Long AD, Emerson JJ: Contiguous and accurate de novo assembly of metazoan genomes with modest long read coverage. Nucleic Acids Res 2016, 44:e147.

Walker BJ, Abeel T, Shea T, Priest M, Abouelliel A, Sakthikumar S, Cuomo CA, Zeng Q, Wortman J, Young SK, Earl AM: Pilon: an integrated tool for comprehensive microbial variant detection and genome assembly improvement. PLoS One 2014, 9:e112963.

Servant N, Varoquaux N, Lajoie BR, Viara E, Chen CJ, Vert JP, Heard E, Dekker J, Barillot E: HiC-Pro: an optimized and flexible pipeline for Hi-C data processing. Genome Biol 2015, 16:259.

Burton JN, Adey A, Patwardhan RP, Qiu R, Kitzman JO, Shendure J: Chromosome-scale scaffolding of de novo genome assemblies based on chromatin interactions. Nat Biotechnol 2013, 31:1119-1125.

Li H, Durbin R: Fast and accurate long-read alignment with Burrows-Wheeler transform. Bioinformatics 2010, 26:589-595.

Parra G, Bradnam K, Korf I: CEGMA: a pipeline to accurately annotate core genes in eukaryotic genomes. Bioinformatics 2007, 23:1061-1067.

G. Benson,"Tandem repeats finder: a program to analyze DNA sequences"Nucleic Acids Research (1999) Vol. 27, No. 2, pp. 573-580.

Price AL, Jones NC, Pevzner PA: De novo identification of repeat families in large genomes. Bioinformatics 2005, 21 Suppl 1:i351-358.

Xu Z, Wang H: LTR_FINDER: an efficient tool for the prediction of full-length LTR retrotransposons. Nucleic Acids Res 2007, 35:W265-268.

Han Y, Wessler SR: MITE-Hunter: a program for discovering miniature inverted-repeat transposable elements from genomic sequences. Nucleic Acids Res 2010, 38:e199.

Edgar RC, Myers EW: PILER: identification and classification of genomic repeats. Bioinformatics 2005, 21 Suppl 1:i152-158.

Bao W, Kojima KK, Kohany O: Repbase Update, a database of repetitive elements in eukaryotic genomes. Mob DNA 2015, 6:11.

Tarailo-Graovac M, Chen N: Using RepeatMasker to identify repetitive elements in genomic sequences. Curr Protoc Bioinformatics 2009, Chapter 4:Unit 4 10.

Burge C, Karlin S: Prediction of complete gene structures in human genomic DNA. J Mol Biol 1997, 268:78-94.

Stanke M, Waack S: Gene prediction with a hidden Markov model and a new intron submodel. Bioinformatics 2003, 19 Suppl 2:ii215-225.

Majoros WH, Pertea M, Salzberg SL: TigrScan and GlimmerHMM: two open source ab initio eukaryotic gene-finders. Bioinformatics 2004, 20:2878-2879.

Blanco E, Parra G, Guigo R: Using geneid to identify genes. Curr Protoc Bioinformatics 2007, Chapter 4:Unit 4 3.

Korf I: Gene finding in novel genomes. BMC Bioinformatics 2004, 5:59.

Keilwagen J, Wenk M, Erickson JL, Schattat MH, Grau J, Hartung F: Using intron position conservation for homology-based gene prediction. Nucleic Acids Res 2016, 44:e89.

Kim D, Langmead B, Salzberg SL: HISAT: A fast spliced aligner with low memory requirements. Nat Methods 2015, 12:357-360.
Pertea M, Pertea GM, Antonescu CM, Chang TC, Mendell JT, Salzberg SL: StringTie enables improved reconstruction of a transcriptome from RNA-seq reads. Nat Biotechnol 2015, 33:290-295.
Campbell MA, Haas BJ, Hamilton JP, Mount SM, Buell CR: Comprehensive analysis of alternative splicing in rice and comparative analyses with Arabidopsis. BMC Genomics 2006, 7:327.
Haas BJ, Salzberg SL, Zhu W, Pertea M, Allen JE, Orvis J, White O, Buell CR, Wortman JR: Automated eukaryotic gene structure annotation using EVidenceModeler and the Program to Assemble Spliced Alignments. Genome Biol 2008, 9:R7.
Lowe TM, Eddy SR: tRNAscan-SE: a program for improved detection of transfer RNA genes in genomic sequence. Nucleic Acids Res 1997, 25:955-964.
Nawrocki EP, Eddy SR: Infernal 1.1: 100-fold faster RNA homology searches. Bioinformatics 2013, 29:2933-2935.
Nawrocki EP, Burge SW, Bateman A, Daub J, Eberhardt RY, Eddy SR, Floden EW, Gardner PP, Jones TA, Tate J, Finn RD: Rfam 12.0: updates to the RNA families database. Nucleic Acids Res 2015, 43:D130-137.
Birney E, Clamp M, Durbin R: GeneWise and Genomewise. Genome Res 2004, 14:988-995.
Marcais, G. et al. MUMmer4: a fast and versatile genome alignment system. PLoS Comput. Biol. 14, e1005944 (2018).
Murray MG, Thompson WF: Rapid isolation of high molecular weight plant DNA. Nucleic Acids Res,1980. 8:4321-5.
Picard: http://sourceforge.net/projects/picard/ .(Picard).
McKenna A, Hanna M, Banks E, Sivachenko A, et al. The Genome Analysis Toolkit: a MapReduce framework for analyzing next-generation DNA sequencing data. Genome Res. 2010 20:1297-303.
Cingolani P, Platts A, Wang le L, et al. A program for annotating and predicting the effects of single nucleotide polymorphisms, SnpEff: SNPs in the genome of Drosophila melanogaster strain w1118; iso-2; iso-3., Fly (Austin). 2012 Apr-Jun;6(2):80-92.
Chen K, Wallis J W, Mclellan M D, et al. BreakDancer: An algorithm for high resolution mapping of genomic structural variation[J]. Nature Methods, 2009, 6(9): 677-681.
Alexander D H, Novembre J, Lange K. Fast model-based estimation of ancestry in unrelated individuals. Genome research, 2009, 19(9): 1655-1664.
Kumar, Sudhir, et al. MEGA X: Molecular Evolutionary Genetics Analysis across Computing Platforms. Molecular biology and evolution 35.6 (2018): 1547-1549.
Purcell S, Neale B, Todd-Brown K, Thomas L, Ferreira MAR, Bender D, Maller J, Sklar P, de Bakker PIW, Daly MJ & Sham PC (2007) PLINK: a toolset for whole-genome association and population-based linkage analysis. American Journal of Human Genetics, 81.
Pfeifer B, Wittelsburger U, Ramosonsins S E, et al. PopGenome: an efficient Swiss army knife for population genomic analyses in R.[J]. Molecular Biology and Evolution, 2014, 31(7): 1929-1936.